Monthly Notices of the ROYAL ASTRONOMICAL SOCIETY

MNRAS **501,** 5257–5273 (2021) doi:10.1093/mnras/staa3634
Advance Access publication 2020 November 21

Intermediate mass black hole formation in compact young massive star clusters

Francesco Paolo Rizzuto,[1★] Thorsten Naab,[1] Rainer Spurzem,[2,3,4†] Mirek Giersz,[5] J. P. Ostriker,[6,7] N. C. Stone,[6,8,9] Long Wang,[10,11] Peter Berczik[2,3,12] and M. Rampp[13]

[1]*Max-Planck Institute for Astrophysics, Karl-Schwarzschild-Str 1, D-85741 Garching, Germany*
[2]*National Astronomical Observatories and Key Laboratory of Computational Astrophysics, Chinese Academy of Sciences, 20A Datun Rd., Chaoyang District, 100101 Beijing, China*
[3]*Astronomisches Rechen-Institut, Zentrum für Astronomie, University of Heidelberg, M"onchhofstrasse 12-14, D-69120 Heidelberg, Germany*
[4]*Kavli Institute for Astronomy and Astrophysics, Peking University, Yiheyuan Lu 5, Haidian Qu, 100871 Beijing, China*
[5]*Nicolaus Copernicus Astronomical Centre, Polish Academy of Sciences, ul. Bartycka 18, PL-00-716 Warsaw, Poland*
[6]*Department of Astronomy, Columbia University, New York, NY 10027, USA*
[7]*Department of Astrophysical Sciences, Princeton University, Princeton, NJ 08544, USA*
[8]*Racah Institute of Physics, The Hebrew University, Jerusalem 91904, Israel*
[9]*Department of Astronomy, University of Maryland, College Park, MD 20742, USA*
[10]*Department of Astronomy, School of Science, The University of Tokyo, 7-3-1 Hongo, Bunkyo-ku, Tokyo 113-0033, Japan*
[11]*RIKEN Center for Computational Science, 7-1-26 Minatojima-minami-machi, Chuo-ku, Kobe, Hyogo 650-0047, Japan*
[12]*Main Astronomical Observatory of Ukrainian National Academy of Sciences, UA-02000 Kiev, Ukraine*
[13]*Max Planck Computing and Data Facility, Gießenbachstr 2, D-85748 Garching, Germany*

Accepted 2020 November 16. Received 2020 November 16; in original form 2020 August 24

ABSTRACT

Young dense massive star clusters are promising environments for the formation of intermediate mass black holes (IMBHs) through collisions. We present a set of 80 simulations carried out with NBODY6++GPU of 10 models of compact $\sim 7 \times 10^4$ $M_\odot$ star clusters with half-mass radii $R_h \lesssim 1$ pc, central densities $\rho_{core} \gtrsim 10^5\,M_\odot\,pc^{-3}$, and resolved stellar populations with 10 per cent primordial binaries. Very massive stars (VMSs) up to $\sim 400\,M_\odot$ grow rapidly by binary exchange and three-body scattering with stars in hard binaries. Assuming that in VMS–stellar black hole (BH) collisions all stellar material is accreted on to the BH, IMBHs with masses up to $M_{BH} \sim 350\,M_\odot$ can form on time-scales of $\lesssim$15 Myr, as qualitatively predicted from Monte Carlo MOCCA simulations. One model forms an IMBH of 140 $M_\odot$ by three BH mergers with masses of 17:28, 25:45, and 68:70 $M_\odot$ within ∼90 Myr. Despite the stochastic nature of the process, formation efficiencies are higher in more compact clusters. Lower accretion fractions of 0.5 also result in IMBH formation. The process might fail for values as low as 0.1. The IMBHs can merge with stellar mass BHs in intermediate mass ratio inspiral events on a 100 Myr time-scale. With 10^5 stars, 10 per cent binaries, stellar evolution, all relevant dynamical processes, and 300 Myr simulation time, our large suite of 80 simulations indicate another rapid IMBH formation channel in young and compact massive star clusters.

Key words: gravitational waves – methods: numerical – stars: black holes – stars: mass-loss – galaxies: star clusters: general.

1 INTRODUCTION

At the end of the 1930s, Oppenheimer & Snyder (1939) suggested that after the exhaustion of all thermonuclear energy sources, heavy stars might collapse. The objects created in these events are stellar black holes (BH) with masses from 5 $M_\odot$ up to about 60 $M_\odot$.[1] A large number of X-ray and optical observations provide solid evidence for the existence of stellar BHs (Webster & Murdin 1972; Remillard & McClintock 2006; Casares & Jonker 2014). Their presence is further confirmed by the recent discovery of gravitational waves generated by BH mergers (Abbott et al. 2016, 2017, 2019a,b). It is also well established that massive galaxies in the local Universe host supermassive black holes (SMBHs) with masses above 10^6 $M_\odot$ (see Kormendy & Ho 2013, for a general review). Before the detection of GW190521 (Abbott et al. 2020) – which was published after the initial submission of this paper – there was no clear observational evidence for the existence of BHs bridging the mass range between stellar and SMBHs. The 150 $M_\odot$ BH observed in the last LIGO/virgo detection, is the merger product between a 66 and an 85 $M_\odot$ BH (Abbott et al. 2020). In general, intermediate mass black holes (IMBHs) could originate from stellar BHs and might be the seeds for SMBHs. Finding them and understanding their formation mechanism is crucial for a full understanding of the BH population in the Universe. There are three theoretical paths for IMBH formation leading to SMBHs discussed in the literature (see reviews Volonteri 2010; Koliopanos 2017, and citations there). In the first scenario, IMBHs form through direct collapse of dense gas at high redshifts. This scenario predicts the formation of IMBHs of 10^4–10^6 $M_\odot$

★ E-mail: rizzuto@MPA-Garching.MPG.DE
† Research Fellow at Frankfurt Institute for Advanced Studies (FIAS).
[1]The lower and upper mass boundaries depend on the stellar evolution model, i.e. details of stellar wind mass-loss and supernova explosions.

(Begelman, Volonteri & Rees 2006; Agarwal et al. 2012; Luo et al. 2020). A second possibility is that IMBHs are the remnants of first-generation (PopIII) stars. These stars formed from zero metallicity gas and are expected to collapse into IMBHs more massive than 100 $M_\odot$ (Madau & Rees 2001; Ryu et al. 2016). A third family of models assumes that IMBHs are generated in dense stellar environments through runaway collisions. Several studies have demonstrated that IMBHs can form through dynamical interactions in dense stellar systems. Those studies include analytical approaches (Begelman & Rees 1978; Stone, Küpper & Ostriker 2017) as well as *N*-body simulations (Portegies Zwart & McMillan 2002; Portegies Zwart et al. 2004; Mapelli 2016; DiCarlo et al. 2020), and Monte Carlo simulations (Freitag, Rasio & Baumgardt 2006; Gürkan, Fregeau & Rasio 2006; Giersz et al. 2015). In particular, the effect of tidal capture of stars by BHs has been discussed in Patruno et al. (2006) for massive star clusters and Stone et al. (2017) for nuclear star clusters.

Several IMBH candidates have been discovered in our galaxy and others nearby. For example, IMBHs have been proposed to explain the nature of ultraluminous X-ray emitters (ULXs). ULXs are extragalactic and off-centre X-ray sources that could be generated by BHs of intermediate mass that accrete gas isotropically below the Eddington rate (Colbert & Mushotzky 1999). Most ULXs observed are, however, more likely generated by smaller objects such as magnetized neutron stars and stellar BHs with super-Eddington accretion (Feng & Soria 2011; Gladstone 2013; Roberts et al. 2016; Kaaret, Feng & Roberts 2017; King & Lasota 2020). This is also confirmed by dynamical evidence (Liu et al. 2013) as well as X-ray pulsations, which indicate the presence of neutron stars (Fürst et al. 2016). Nevertheless, there exists a group of hyperluminous X-ray sources (HLXs) that might be labourious to explain by super-Eddington accretion since their luminosity exceeds $\sim 10^{41}$ erg s^{-1}. Probably the best IMBH candidate known so far is HLX-1. This HLX is believed to host an IMBH because it has an X-ray luminosity of 1.1×10^{42} erg s^{-1} (Farrell et al. 2009). This luminosity would imply a mass of 500 $M_\odot$ even assuming an accretion rate 10 times larger than the Eddington limit (Farrell et al. 2009). The mass estimates of the BH associated with HLX-1 is estimated between 3.0×10^3 and 3.0×10^5 $M_\odot$ (see review Mezcua 2017, and references therein). Other notable sources in the same category are NGC 5252 and NGC 2276-3C, which have been estimated to host IMBHs of $\sim 10^5$ (Kim et al. 2020) and $\sim 5 \times 10^4$ $M_\odot$ (Mezcua et al. 2013, 2015), respectively. Another HLX is M82 X-1. This X-ray source is associated with a young massive star cluster (YMSC; MGG-11) in the starburst galaxy M82 (Matsumoto & Tsuru 1999; Kaaret et al. 2001). First observations have suggested that it is generated by a BH with a mass of 200–5000 $M_\odot$ (Kaaret et al. 2001; Matsumoto et al. 2001; Strohmayer & Mushotzky 2003; Patruno et al. 2006). A more recent analysis indicates the presence of an IMBH, estimating its mass to $\sim$400 $M_\odot$ (Pasham, Strohmayer & Mushotzky 2014). However, M82 X-1 could still be a stellar mass BH with super-Eddington accretion (Brightman et al. 2016).

Globular clusters have been popular targets for the search of IMBHs. Due to their high central density, and possibly even higher density at formation (Lahén et al. 2019), they provide a promising environment for the formation of IMBHs through runaway core collapse and collision. Many studies have attempted to detect IMBHs in globular clusters through their accretion signatures. However, so far G1 in M31 is the only globular cluster detected in X-rays (Pooley & Rappaport 2006; Kong 2007). This signal might be generated by an IMBH with a mass of about 2×10^4 $M_\odot$ (Gebhardt, Rich & Ho 2002, 2005). A recent observational study reports the lack of IMBHs accretion signatures in 19 globular clusters located in the early-type galaxy NGC 3115 (Wrobel & Nyland 2020). Observations based on kinematic measurements might suggest the presence of IMBHs in globular clusters such as M15 (Bahcall & Wolf 1976; Peterson, Seitzer & Cudworth 1989), ω Centauri (Noyola, Gebhardt & Bergmann 2008; Noyola et al. 2010), and NGC 1904 and NGC 6266 (Lützgendorf et al. 2013). However, these observations could also be explained by a central concentration of compact objects (Baumgardt et al. 2003; van den Bosch et al. 2006; Baumgardt, Sollima & Hilker 2020). Measurements of pulsar accelerations indicate that the globular cluster 47 Tucanae might host an IMBH of 2300^{+1500}_{-850} $M_\odot$ (Kızıltan, Baumgardt & Loeb 2017). Another study suggests that current observations of pulsar accelerations are insufficient to confirm the presence of an IMBH in 47 Tucanae, they can only be used to estimate an upper limits on its mass (Abbate et al. 2018).

Dwarf galaxies are very promising systems for IMBH searches. NGC 4395 seems to be one of the most plausible candidates for an active and central IMBH. Observations of the central stellar velocity dispersion reveal a value of 30 km s^{-1} (Filippenko & Ho 2003), suggesting an IMBH mass of $\sim 10^5$ $M_\odot$. Further measurements based on the broad profile of the H β line, from X-ray variability (Filippenko & Ho 2003), reverberation mapping (Peterson et al. 2006; Edri et al. 2012), and integral field kinematics (den Brok et al. 2015) indicate a mass in the range between 10^4 and 10^5 $M_\odot$. Also our Galaxy might host an IMBH in the vicinity of the Galactic Centre as suggested by recent high-resolution molecular line observations that indicate the presence of a $\sim 10^4$ $M_\odot$ candidate BH in the central region of the Milky Way (Takekawa et al. 2020).

In this paper, we study IMBH formation paths in young concentrated star clusters with numerical simulations. The simulations incorporate detailed models for single and binary stellar evolution as well as mass-loss due to stellar winds. In Section 2, we describe the *N*-body code used to simulate star cluster evolution and focus on the description of the adopted stellar evolution and collision models. In Section 3, we describe the initial conditions for our models. The results of our simulations are discussed in Section 4. In Section 5, we compare these results with previous studies. In the final section, we summarize the main points of this paper.

2 THE METHOD

To investigate the possible formation of IMBHs in massive star clusters, we generated initial conditions for 80 isolated systems[2] using MCLUSTER (Küpper et al. 2011). The systems were set-up with two different half-mass radii and various central concentrations. Each initial condition is evolved for a few hundred million years employing NBODY6++GPU (Wang et al. 2015; Wang et al. 2016), a direct *N*-body simulation code designed to follow the dynamical and stellar evolution of individual stars and binaries.

2.1 NBODY6++GPU

NBODY6++GPU[3] is a high-precision direct *N*-body simulation code based on the earlier *N*-body codes NBODY1-6 (Aarseth 1999) and NBODY6++ (Spurzem 1999). For time integration, it uses the Hermite scheme. This together with the hierarchically blocked variable

[2]We study clusters in isolation to investigate internal dynamical effects without possible external influences.

[3]Link to repository: http://silkroad.bao.ac.cn/repos/Nbody6++GPU-Aug2020/.

time-step scheme allows an efficient parallelization of the code for massively parallel supercomputers (since NBODY6++); gravitational forces between particles are offloaded to graphics processing units (GPUs), used for high-performance general purpose computing (NBODY6++GPU; Wang et al. 2015). The parallelization is achieved via MPI and OpenMP on the top level, distributing work within a group of particles due for time integration, and efficient parallel use of GPU cores at the base level (every MPI process using a GPU), for computing the gravitational forces between particles. The GPU implementation in NBODY6++GPU provides a significant performance improvement, especially for the long-range (regular) gravitational forces (see Nitadori & Aarseth 2012; Wang et al. 2015, 2016).

The code accurately computes the evolution of binaries, multiples, and close encounters between them and single stars and between multiple systems, using the Kustaanheimo–Stiefel (KS; Kustaanheimo & Stiefel 1965) regularization with the classical chain algorithm by Mikkola & Aarseth (1998). It also follows single and binary stellar evolution based on the SSE and BSE recipes by Hurley (see Section 2.2), including also rapid tidal circularization for binaries with small pericenters and tidal captures according to the prescription given in Mardling & Aarseth (2001), which is based on the previous work of Press & Teukolsky (1977), Lee & Ostriker (1986), and Mardling (1996). The integrator fully resolves orbits and dynamical evolution of binaries, even during phases of mass-loss or when one of the two stars undergoes a supernova explosion. The binary orbit is adjusted to the corresponding loss of mass, energy, and angular momentum with appropriate time stepping; in case of a supernova explosion, it is always ensuring that the remnant and its companion leave the explosion with the corrected orbital positions and velocities.

In the implementation used for this study, we compute the gravitational wave energy loss of hard binaries according to the orbit averaged approximation of Peters & Mathews (1963), using the average change of energy and angular momentum per orbit from their work. At each KS integration time-step, which is much smaller than the orbital time, we apply a corresponding fractional loss of energy and angular momentum. This allows for the proper representation of the evolution of gravitational radiation driven shrinking and circularization of the orbit, until the time-scale of orbit shrinking becomes comparable to the orbital time. When this happens, the time to final coalescence is very short and we assume coalescence. Relativistic kicks are not included in the current implementation.

The publicly available code NBODY6++GPU has been significantly upgraded in three respects:

(i) For collisions between a compact remnant and a main-sequence star or red giant, a free parameter f_c is introduced, which described the mass-loss from the system in the process. The previous NBODY6 versions used only $f_c = 1$, i.e. no mass-loss in the process (see equations 1 and 2 above). Routine involved: `coal.f`.

(ii) Simultaneous treatment of classical tidal interactions (Roche lobe overflow) and post-Newtonian orbit-averaged orbit shrinking due to gravitational wave emission has been made possible. Both are treated technically in a similar way, and can now be switched on together. Routines and parameters involved: `ksint.f`, `kstide.f`, `tides3.f`, `KZ(27)`.

(iii) Strongly bound binaries of two compact objects, which are subject to post-Newtonian relativistic energy loss are prevented from chain integration: they are treated exclusively in the two-body KS integrator. Routine involved: `impact.f`.

2.2 Stellar evolution

The simulations in this paper were performed with the same stellar evolution models as the DRAGON simulations presented in Wang et al. (2016). Stellar evolution is implemented using analytical fits to the models of Eggleton, Fitchett & Tout (1989, 1990) developed by Hurley, Pols & Tout (2000) for single stars (SSE) and by Hurley, Tout & Pols (2002) for binary stars (BSE). A few updates were included for strong kicks at neutron star birth (Hobbs et al. 2005) and for fallback and more massive BH formation of massive stars at low metallicities (Belczynski, Kalogera & Bulik 2002).

The code is able to follow the main properties of single stars (such as radius, mass, luminosity, and core mass) from the zero-age main sequence to the remnant stage. This also includes mass-loss due to stellar winds for a wide range of masses and metallicities. As long as the orbit of a binary star is wide enough, the evolution of each star is assumed not to be affected by its companion and just the single-star tracks are used. However, if one of the two stars is losing mass by a stellar wind, the companion has the chance to accrete material and deviate from its standard evolution. For close enough orbits either star might fill its Roche lobe leading to mass transfer. For these cases, the code computes the accretion rate as a function of the masses, the radii, the stellar types, and the separation of the donor and the accretor, ensuring that it never exceeds 100 times the Eddington limit. If the matter ejected by a star is not entirely absorbed by its companion it might accumulate in a common envelope around the two stars. All the above effects: mass transfer, Roche phase, and common envelope evolution have significant consequences for the orbit and stellar properties of the binary and are included in the simulations based on the models of Tout et al. (1997).

Our stellar evolution treatment does not include the latest stellar wind prescriptions. With our recipes, an isolated star, independently on its initial mass, can never form a BH with a mass larger than 30 $M_\odot$. On the contrary, according to most updated models (Vink, de Koter & Lamers 2000; Gräfener & Hamann 2008; Vink et al. 2011; Sander & Vink 2020), a massive star with low zero-age main-sequence metallicity is expected to lose little mass through stellar winds. At the same time, non-rotating metal-poor stars in the mass range between 70 and 140 $M_\odot$ are expected to end their life as pulsational pair-instability supernovae (PPISN); consequently, they are expected to eject a large fraction of their masses leaving a BH remnant with a maximum mass of about 40–50 $M_\odot$ (Heger et al. 2003; Woosley 2017). Metal-poor stars, with mass at least 140 $M_\odot$ up to roughly 260 $M_\odot$, will experience a single violent pulse that disrupts the entire star as a pair-instability supernova (PISN); no remnant is left behind. Our simulations do not include treatments for PPISN and PISN. The absence of these two effects together with the conservative stellar winds model adopted, might have altered the dynamical processes that lead to the formation of the IMBHs. Therefore, with an updated prescription of stellar winds and with treatments for PPISN and PISN, we might obtain different masses of the IMBHs.

In dense environments, where stellar collision rates are high, runaway collisions (Lee 1987; Quinlan & Shapiro 1987, 1989, 1990) can generate stars above the maximum initial mass function (IMF) mass of 100 $M_\odot$ (Portegies Zwart & McMillan 2002; Gürkan, Freitag & Rasio 2004; Portegies Zwart et al. 2004; Mapelli 2016; DiCarlo et al. 2020; Wang et al. 2020) for which we use the term 'very massive stars' (VMS). To track the evolution of VMSs, in the absence of observational constraints, we extrapolate our stellar evolution model to stars with arbitrary large masses. Therefore, VMSs are affected by strong stellar wind mass-loss and lose a significant fraction of

their mass during their lifetime. In our stellar evolution framework, it is therefore impossible to form massive BHs from direct stellar collapse. In fact, with the adopted stellar evolution recipes, even an isolated star with a mass of 500 $M_\odot$ generates a BH of only about 30 $M_\odot$.

It is worth mentioning that theories of stellar evolution predict that a low metallicity star more massive than 260 $M_\odot$ collapses directly into a BH without significant mass-loss in supernova explosions (see Woosley & Heger 2015, and citations therein). However, it is important to take into account the complex stellar structure acquired by VMSs during merger events. A detailed computation of the evolution of collision products shows that VMSs formed through runaway collisions and tidal capture are dominated by mass-loss from stellar winds that drastically reduce their final remnant mass (Glebbeek et al. 2009).

Despite using a stellar evolution model where stellar winds strongly affect the most massive stars and direct collapse into IMBHs is not possible, we can still form BHs more massive than 100 $M_\odot$ through BH–BH and BH–star collisions. We will show, in the next sections, that BH–VMS collisions provide the main channel for the formation of IMBHs. In other words, our results show that BHs with a mass above 100 $M_\odot$ form when a stellar BH merges with a VMS in agreement with previous works (Giersz et al. 2015; Mapelli 2016). Runaway tidal captures (Stone et al. 2017) can also produce IMBHs.

2.3 Collisions

The outcome of a collision depends on the relative velocity, the relative sizes, and the internal structure of the two colliding objects. In general, full 3D radiation magnetohydrodynamical simulations are required to robustly determine the properties of the final object (such as mass, size, and internal structure). In the absence of results covering the full parameter space, NBODY6++GPU adopts a simplified treatment. If a collision does not involve red giants, the two objects are merged when the radii of two colliding objects overlap and the merger of the two masses is assumed to be instantaneous. If M_1 and M_2 are the masses of two stars or two compact objects (BHs, neutron stars, white dwarf, etc.), the final object will have a mass M_f equal to

$$M_\mathrm{f} = M_1 + M_2. \quad (1)$$

Otherwise, if M_1 is the mass of a compact object and M_2 is the mass of a star, the final mass of the compact object, M_f, is given by

$$M_\mathrm{f} = M_1 + f_\mathrm{c} \times M_2, \quad (2)$$

where $0 < f_\mathrm{c} < 1$ represents the amount of stellar material falling back and accreted on to the BH during the coalescence.

The value of f_c has been debated in the literature only for tidal disruption events involving an SMBH and a low-mass star ($M_\mathrm{BH} >> M_*$). Several analytical and numerical studies indicate $0.25 < f_\mathrm{c} < 0.5$ (Shiokawa et al. 2015; Law-Smith, Guillochon & Ramirez-Ruiz 2019; Bonnerot & Lu 2020; Lu & Bonnerot 2020) in agreement with a recent observational work (Wen et al. 2020). The latter shows that in some tidal disruption events, f_c can be measured, and has a value in the range between 0.2 and 0.5. Another work explores the scenario in which most of the stellar material is ejected in an outflow during the tidal interaction with the SMBH arguing that $f_\mathrm{c} < 0.1$ is not impossible (Metzger & Stone 2016).

Our case of interest ($M_\mathrm{BH} \lesssim M_*$) is more uncertain and needs future investigation. In our theoretical work, we treat f_c as a free parameter and explore scenarios with $f_\mathrm{c} = 0.1$, 0.5, and 1.0 (see Fig. 9). Here, we anticipate that the main IMBH formation mechanism proposed in this paper is strongly suppressed when $f_\mathrm{c} = 0.1$.

Collisions involving a giant or giant-like star with a dense core and a large envelope are assumed to lead to common-envelope evolution. In this situation, the envelope of the red giant wraps around both cores of the two objects.[4] The outcome depends on the orbital energy of the two cores as well as the binding energy of the envelope. If the latter is too low, the wrapper might be removed from the system before the two cores merge, leaving behind a binary composed of the appropriate remnants. Otherwise, the two cores are destined to spiral into each other. The final mass depends on their relative density. If they are of different compactness, equation (2) applies, otherwise the code uses (1).

When two stars of similar compactness merge, we assume that they coalesce and mix completely. As a consequence, the final star can be rejuvenated since the core of the final object absorbs new fuel. This phenomenon is well established as it explains the peculiar evolution of blue stragglers as the product of binary evolution and direct stellar collisions (Davies, Piotto & de Angeli 2004; Davies 2015; Smith & Tombleson 2015). This rejuvenation procedure also applies to main-sequence (MS) stars, even if they are assumed to have no core. For more details, see section 2.6.6 of Hurley et al. (2002).

When two BHs (or neutron stars) form hard binaries, gravitational wave emission is computed with the Peters & Mathews formulae (Peters & Mathews 1963). The semimajor axes and the eccentricities are then changed according to the amount of gravitational wave energy emitted.

3 INITIAL CONDITIONS

We created initial conditions for 10 isolated[5] star cluster models following a King density profile (King 1966) with two different half-mass radii and five different central densities varying the dimensionless central potential parameter $6 \leq W_0 \leq 10$. For a fixed value of the half-mass radius, the central density increases with increasing W_0[6] (see Fig. 1). All simulated clusters were initialized with a very low metallicity of $Z = 0.0002$ and $N = 1.1 \times 10^5$ stars sampled from a Kroupa IMF (Kroupa 2001) as zero-age main-sequence stars in a mass range of 0.08–100 $M_\odot$ (see Fig. 2). No primordial mass segregation was included. Because of computing performance limit, we did not use very high primordial binary fraction as suggested by some observations (Sana et al. 2012; Moe & Di Stefano 2017). Our clusters are initialized with 10 000 initial binaries (a primordial binary fraction of 10 per cent) with a uniform semimajor axis distribution on a logarithmic scale from 0.001 to 100 au,[7] a uniform distribution of mass ratios, and a thermal distribution of eccentricities. With this binary distribution, about 30 per cent of the primordial binaries are weak and they dissolve in the cluster at the beginning of the simulation. For each initial condition parameter set,

[4] For main-sequence stars and BHs, the core mass coincides with the mass of the objects itself.

[5] According to the code, a star escapes from an isolated cluster when its energy is larger than zero, $E > 0$ and its distance from the centre is larger than $30R_\mathrm{h}$.

[6] The exact definition of the parameter $W_0 = \frac{\psi(0)}{\sigma^2}$ where $\psi(0)$ is the potential at the centre of the cluster and σ^2 is a parameter connect to the velocity dispersion defined from the distribution function; see King (1966), section 3 and Heggie & Hut (2003), chapter 8 for more details.

[7] To generate the semimajor axis distribution, we impose the further constraint that the initial semimajor axes of each binary are larger than the sum of the diameters of the two stars.

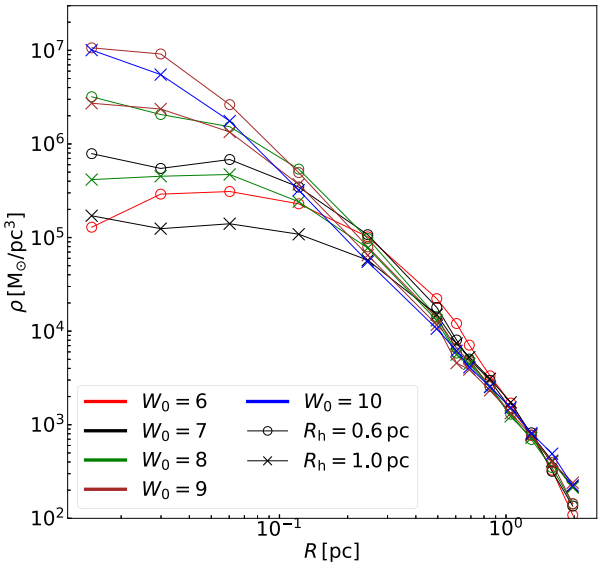

Figure 1. Initial density distributions for the cluster simulations presented in Table 1, initialized with a King density profile (King 1966) with two half-mass radii and different central potential parameters W_0 (different colours). Systems with $R_h = 0.6$ pc are represented with filled circles while models with $R_h = 1.0$ pc are represented by crosses.

we created eight realizations with different random number seeds. In Table 1, we list the initial conditions parameters of the 10 models including the number of realizations that lead to the formation of IMBHs and their respective masses. All simulations were run for more than 300 Myr up to 500 Myr.[8]

The clusters studied in this work are initialized with a low metallicity value (about two orders of magnitude lower than the solar metallicity), they are rather compact with high initial central densities and small half-mass radii. For this reason, they do not resemble the typical properties of YMSCs in the observable range. The latter have higher, and closer to solar, metallicity and are typically less compact; observed YMSCs with masses similar to our models have virial radii typically in the range from 3 to 30 pc (Portegies Zwart, McMillan & Gieles 2010). Even considering the expansion driven by stellar and dynamical evolution, our less compact systems would have a virial radius from 2 to 30 times smaller than most of the observed massive clusters.

However, it is still possible to find a few compact YMSCs in the local Universe. An example is Westerlund 1, which has a virial radius of $\sim$1.7 pc (our $R_h = 0.6$ pc model at the same age has a virial radius of about 1.15 pc) and a mass $\sim 6 \times 10^4$ M$_\odot$ (Mengel & Tacconi-Garman 2007; Portegies Zwart et al. 2010). Another exception is MGG-11 in M82. This cluster has a half-light radius of about 1.2 pc and a mass of about 3.50×10^5 M$_\odot$ (McCrady, Gilbert & Graham 2003).

Our models start with velocity dispersions σ between 15 and 12 km s^{-1} (see Table 1) that drop to values between 6.1 and 5.3 km s^{-1} after 300 Myr as shown in Table 2. We also show the half-mass radius, the relaxation time, the number of particles, and fraction of total mass left in the cluster after 300 Myr. It is interesting to notice that R06W9, which formed the most massive IMBHs, after 300 Myr has a dispersion velocity and half-mass radius very similar to the least compact model R1W7 (see Table 2), which never formed a BH more massive than 100 M$_\odot$. The velocity dispersions shown in Table 2 are approximately in the same range of the observed values of the globular clusters in our Galaxy (Baumgardt & Hilker 2018). However, our clusters are too small to resemble the initial conditions of present-day globular clusters and estimating the particle number of our clusters at late times using equation (22) in Gieles, Heggie & Zhao (2011), our systems might not survive for 10 Gyr even if we assume no external tidal forces.

We have chosen these initial conditions mainly to investigate the formations of IMBHs through dynamical interactions. Nevertheless, our theoretical models might approximate the properties of clusters formed at a high redshift, which may be located around any galaxy in the LIGO/Virgo sensitivity volume ($\sim$1 Gpc^3).

4 RESULTS

The dynamical evolution of a star cluster is dominated by two-body relaxation on time-scales longer than the relaxation time (Spitzer 1987):

$$t_{\rm rh} = \frac{0.138 N^{1/2}}{\ln \Lambda} \left(\frac{R_{\rm h}^3}{G\bar{m}} \right)^{1/2}. \quad (3)$$

Here, N is the number of stars in the cluster, R_h is the half-mass radius, and $\bar{m}$ is the average star mass of the cluster and the argument of the Coulomb logarithm is $\Lambda = \gamma N$. Numerical experiments indicate a value for the parameter $\gamma = 0.11$ for single-mass systems (Giersz & Heggie 1994) and $\gamma = 0.02$ for multimass stellar systems (Giersz & Heggie 1996). We have used equation (3) to estimate half-mass relaxation times of 56 and 120 Myr for systems with 0.6 and 1 pc half-mass radii, respectively (see Table 1).

The internal structure of star clusters evolves into a dense hot core and an extended halo. Since bound self-gravitating systems have negative heat capacity (Lynden-Bell & Wood 1968; Lynden-Bell 1999), the centre will keep releasing energy to the outer part and contracts in a core collapse. In an isolated equal-mass system, this happens on the order of $15t_{\rm rh}$ (Cohn 1980). In clusters with a broad mass spectrum, low-mass stars gain kinetic energy when interacting with massive stars; the former tends to expand their orbits, while the latter tends to lose kinetic energy and segregate to the central part of the cluster. In this case, core collapse is driven by the amassing of heavy stars in the core that typically occur in a time-scale of the order of the segregation time (Spitzer & Hart 1971; Portegies Zwart et al. 2004):

$$t_{\rm s} = \frac{\bar{m}}{M_{\rm max}} \frac{0.138N}{\ln(0.11M/M_{\rm max})} \left(\frac{R_{\rm h}^3}{GM} \right)^{1/2}, \quad (4)$$

where $M_{\rm max}$ is the mass of the most massive object in the cluster and M is the total mass of the cluster. Consequently, multimass clusters undergo core collapse in much shorter time then single-mass systems. According to equation (4), our $R_h = 0.6$ pc and $R_h = 1.0$ pc models are expected to experience mass segregation at $t_s \sim 1.4$ and 3 Myr, respectively (see Table 1).

Core collapse leads to dramatic growth in the central density which in turn triggers violent few-body interactions between single stars and binaries, either primordial or dynamically formed. By means of this interaction, binary stars release energy in the core and balance the loss of energy from the centre preventing the core to collapse further (see Heggie & Hut 2003, and references therein).

We show in Fig. 3 that the most massive stars formed in each simulation (red crosses) consistently have masses much higher than the initial limit of 100 M$_\odot$. These systems have formed by mergers

[8]We evolved for longer time the clusters that formed an IMBH to check whether the BH would keep growing in mass or it would be ejected from the cluster through a strong interaction.

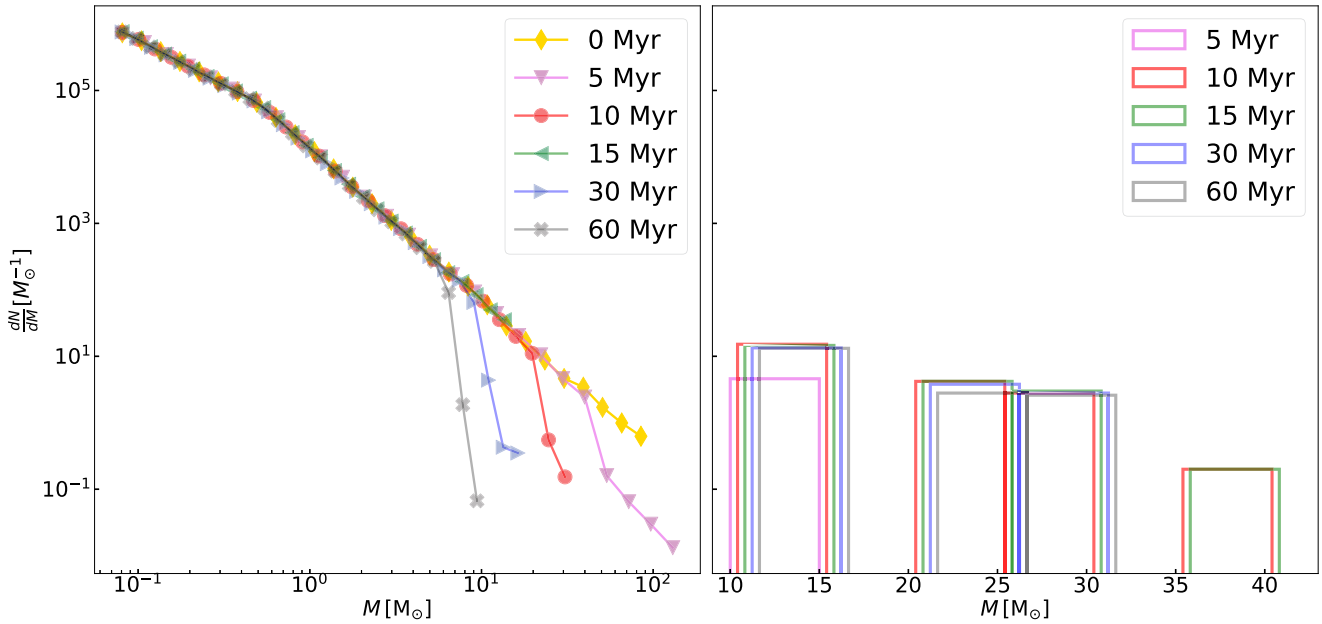

Figure 2. Left-hand panel: Stellar mass function (the mass function is computed including all stellar types apart from compact objects) at 0, 5, 10, 15, 30, and 60 Myr. Right-hand panel: Compact objects mass function (the mass function includes only BHs, all neutron stars are ejected from the cluster due to supernovae kick) at 0.0, 5, 10, 15, 30, and 60 Myr.

Table 1. Model parameters of the cluster simulations: r_c: initial core radius; ρ_c: initial central density; W_0: central potential parameter for the King density profile (King 1966); R_h: half mass radius; σ: dispersion velocity; t_{rh}: half-mass relaxation time computed using equation (3) with $\gamma = 0.02$; t_s: segregation time-scale for 100 $M_\odot$ objects computed using equation (4); f_c: fraction of mass absorbed by a compact object during a direct collision with a star; #IMBH: number of BHs with masses $\geq$100 $M_\odot$ formed out of eight realizations; M_{IMBH}: IMBH masses; t_{form}: IMBHs formation times; M_*/M_{IMBH}: the total stellar mass accreted by the IMBH divided by its final mass.

Model name	r_c (pc)	ρ_c ($M_\odot$ pc^{-3})	W_0	R_h (pc)	σ (km s^{-1})	t_{rh} (Myr)	t_s (Myr)	f_c	#IMBH	M_{IMBH} ($M_\odot$)	t_{form} (Myr)	M_*/M_{IMBH}
R06W9F01	0.04	3.0×10^7	9	0.6	15	56	1.4	0.1	0/8	–	–	–
R06W9F05	0.04	3.0×10^7	9	0.6	15	56	1.4	0.5	2/8	138, 110	5.5, 6.3	79 per cent, 81 per cent
R06W6	0.19	1.1×10^5	6	0.6	15	56	1.4	1.0	4/8	307, 151, 138, 122	8.6, 83.9, 6.4, 8.4	86 per cent, 26 per cent, 72 per cent, 80 per cent
R06W7	0.13	5.0×10^5	7	0.6	15	56	1.4	1.0	2/8	148, 147	22.9, 8.2	76 per cent, 87 per cent
R06W8	0.06	3.0×10^6	8	0.6	15	56	1.4	1.0	3/8	336, 171, 110	6.6, 12.3, 8.1	98 per cent, 87 per cent, 77 per cent
R06W9	0.04	3.0×10^7	9	0.6	15	56	1.4	1.0	3/8	355, 349, 120	8.57, 8.19, 16.3	81 per cent, 89 per cent, 73 per cent
R1W7	0.2	1.0×10^5	7	1.0	12	120	3.0	1.0	0/8	–	–	–
R1W8	0.11	4.0×10^5	8	1.0	12	120	3.0	1.0	0/8	–	–	–
R1W9	0.05	3.0×10^6	9	1.0	12	120	3.0	1.0	1/8	239	16.4	92 per cent
R1W10	0.03	1.8×10^7	10	1.0	12	120	3.0	1.0	2/8	133, 110	13.2, 7.8	83 per cent, 83 per cent

Table 2. Half-mass radius R_h , dispersion velocity σ, half-mass relaxation time t_{rh}, number of particles N, and final to initial total cluster mass ratio M_f/M_i after 300 Myr; where M_i is the initial mass of the cluster, while M_f is the final mass of the cluster.

Model name	R_h (pc)	σ (km s^{-1})	N	t_{rh} (Myr)	M_f/M_i
R06W6	2.45	6.09	106 800	519	0.695
R06W7	2.57	5.93	106 400	573	0.693
R06W8	2.69	5.71.	106 700	620	0.690
R06W9	2.82	5.56	105 900	671	0.688
R1W7	2.92	5.48	107 800	772	0.702
R1W8	3.11	5.41	107 500	820	0.698
R1W9	3.24	5.33	107 200	860	0.692
R1W10	3.41	5.25	106 700	894	0.689

of lower mass main-sequence stars. As described in Section 2.2, our stellar evolution recipes do not allow for the formation of a stellar BH more massive than 30 $M_\odot$. Nevertheless, Fig. 3 demonstrates that several cluster systems generate BHs more massive than 100 $M_\odot$. In our framework, the only possible way to grow such a massive object is through dynamical interactions (see Section 4.1).

The likelihood to form a VMS by mergers or tidal captures seems to be correlated with the compactness of the cluster. Only six star clusters with $R_h = 1.0$ pc form stars with masses above 200 $M_\odot$, while clusters with $R_h = 0.6$ pc form 15 stars more massive than 200 $M_\odot$ (see Fig. 3). Those stars play an important role in the production of IMBHs as their collisions with stellar BH are the main IMBH formation channel. Such a formation path for IMBHs has been predicted by Monte Carlo models (Giersz et al. 2015) and is discussed in more detail below.

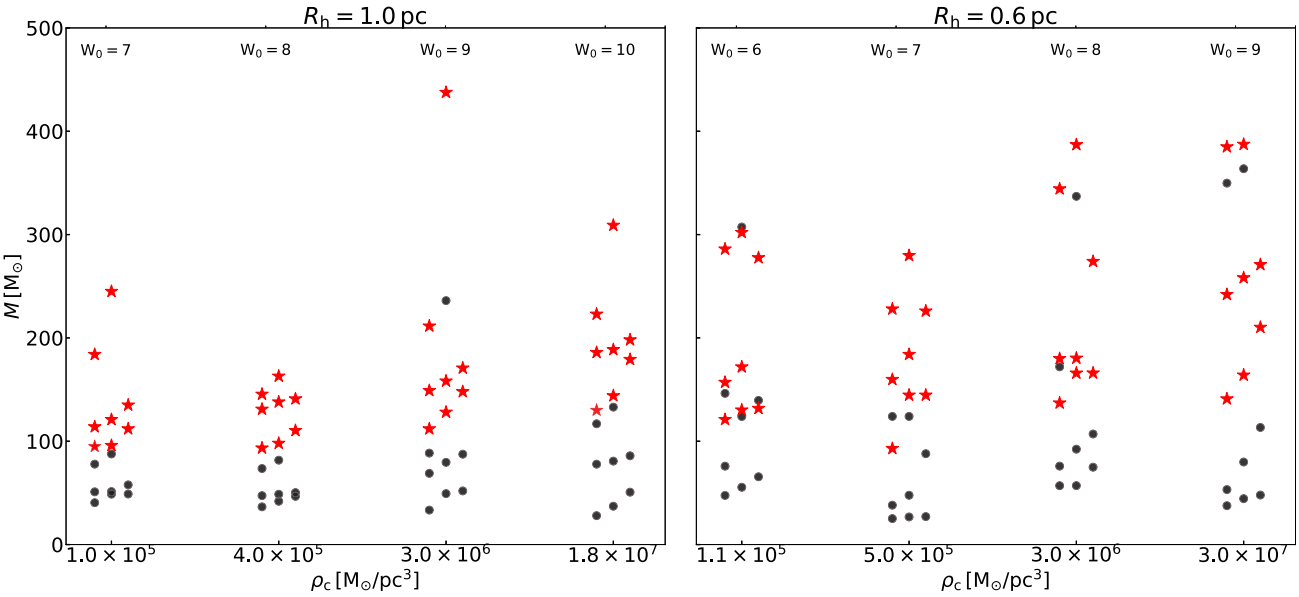

Figure 3. Peak masses of the VMS formed by collisions (red stars) and BHs (black circles) for all simulations with $f_c = 1$ sorted by initial core density (see Table 1). The left-hand (right-hand) panel shows models with a half-mass radius of $r_h = 1$ pc ($r_h = 0.6$ pc). Each model has eight realizations (plotted with random offset). W_0 does not seem to have a strong impact on the final BH mass. A larger cluster half-mass radius apparently makes BH mass growth less likely (left-hand panel).

4.1 Intermediate mass black hole formation

Fig. 4 illustrates how IMBHs of a few hundred solar masses are typically generated in our simulations. The formation consists of three main steps. First, a sequence of binary stellar collisions, triggered by triple interactions and hyperbolic collisions generates a VMS which can live up to 10 Myr due to mixing rejuvenation (see Section 2.2). Second, in a merger with a stellar mass BH, a great part of the mass of the VMS is absorbed by the BH. In a third step, the IMBH can grow in mass by collisions with other stellar BHs. Our results indicate that, for our models, the dominant process for the formation of IMBHs is a collision between a VMS and a stellar mass BH. This type of collisions can lead to the formation of IMBHs of up to 350 $M_\odot$ within the first 10 Myr of cluster evolution. Our simulations also indicate that after all massive stars disappear from the cluster, the IMBH can still grow moderately in mass by merging with other stellar mass BHs and other types of stars.

The IMBH formation scenario shown in our work might change with the inclusion of PPISN, PISN prescriptions, and updated stellar wind recipes. Although the inclusion of these treatments should not prevent the dynamical formation of IMBHs shown by our simulations, further investigation in this direction must be done in order to understand how these effects can influence our final outcome.

Here, it is important to mention that relativistic kicks are not implemented in our simulations. Theoretically, an IMBH could be ejected from the cluster by gravitational wave recoil after a collision with one of the stellar mass BHs left in the system. However, except for of the simulation illustrated in Fig. 5, we expect the clusters to have good chances of retaining their IMBHs as the IMBH–BH mass ratio is small (Fig. 4 shows the typical mass ratio in a collision between an IMBH and a stellar BH: $\frac{m_{\rm BH}}{M_{\rm IMBH}} \approx \frac{20}{300} \approx 0.067$). According to Campanelli et al. (2007), Baker et al. (2008), Lousto & Zlochower (2009), Kulier et al. (2015), Morawski et al. (2018), and Zivancev, Ostriker & Kupper (2020), the maximum gravitational velocity kick is $\sim(0.067)^2 \times 4000\ {\rm km\,s^{-1}} \sim 18\ {\rm km\,s^{-1}}$ and it is smaller than the cluster escape velocity in the core that is about 25 $\rm km\,s^{-1}$.

Our most compact models register about 300 collisions within 300 Myr, 40 per cent of which happen in the first 15 Myr. Most of these collisions are triggered by three-body scattering events[9] between a hard binary and a third particle. These interactions have the overall effect of increasing the binding energy of the binaries and they can also raise their eccentricity (Heggie 1975; Nash & Monaghan 1978; Hut & Bahcall 1983; McMillan & Hut 1996). In general, when the distance of closest approach of the third object is comparable with the semimajor axis of the hard binary, the net effect of the interaction is to harden the binary (Heggie 1975; Nash & Monaghan 1978; Hut & Bahcall 1983; McMillan & Hut 1996). On the other hand, when the pericenter of the intruder is considerably larger than the size of the binary, the interaction is approximately adiabatic, and there is no exchange of energy between the binary and the intruder. However, the binary and the third object can form a hierarchical triple, which excites the eccentricity of the inner binary to values close to unity (Kozai 1962; Lidov 1962) and induces the two components of the binary to merge. Fig. 6 illustrates the dynamical process leading to the collision of two massive stars with 170 and 80 $M_\odot$, respectively. The 170 $M_\odot$ star approaches a binary (0.1–80 $M_\odot$) in a hyperbolic orbit (left-hand panel); during the interaction, the intruder forms a hard binary with the 80 $M_\odot$ star, while the lightest component escapes in a wider orbit (panel 2). Due to the perturbation of the third object, the eccentricity of the new 170 and 80 $M_\odot$ binary increases from 0.002 to 0.45 and the two massive stars crash into each other. Fig. 6 also shows that the colliding objects do not necessarily need to be in a primordial binary. Exchanges are very frequent in triple interactions. Typically, encounters leading to exchange increase the mass of the components of a hard binary because the lowest mass is most likely to escape (see Heggie & Hut 2003, and references therein).

[9] About 2 per cent of collisions are hyperbolic.

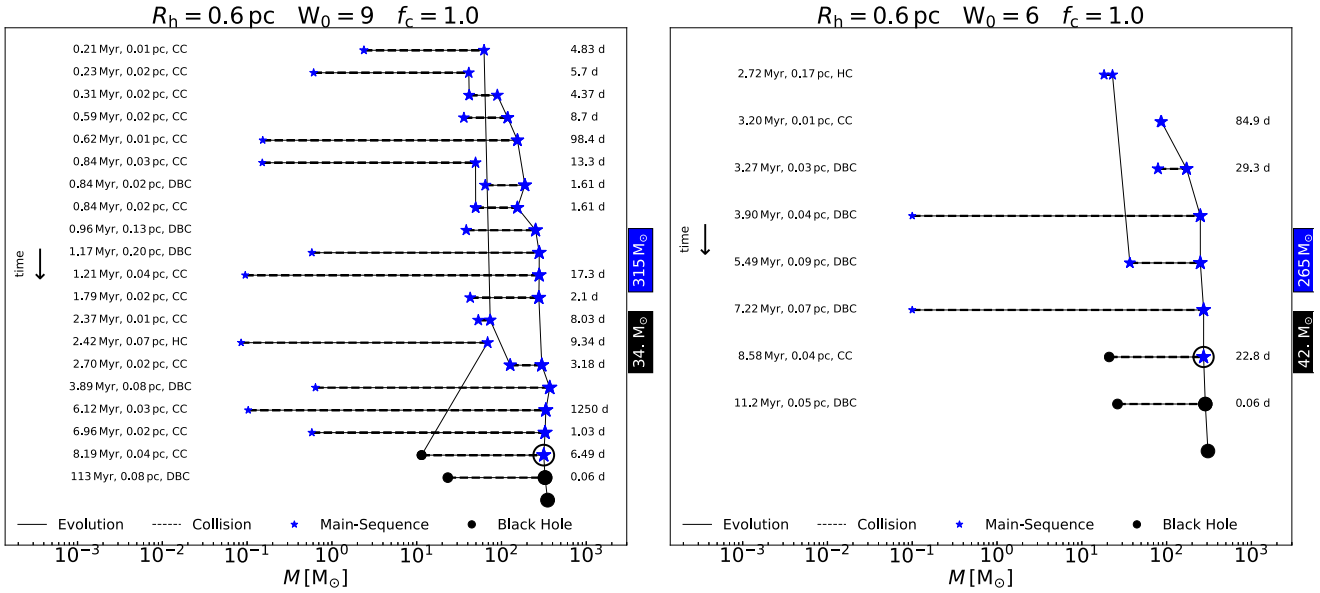

Figure 4. The left-hand panel shows – from top to bottom – the formation history of an IMBH in a simulation with $W_0 = 9$, $R_h = 0.6$ pc, and $f_c = 1.0$. A massive main-sequence star (MS, blue) grows by mergers (dashed horizontal lines) with other MS stars and evolves into ≈300 $M_\odot$ MS star colliding with a 10 $M_\odot$ BH, forming an IMBH about 8.2 Myr after the start of the simulation (the open black circle indicates the collision that leads to the formation of the IMBH). At about 113 Myr, the IMBH collides with another BH. In a similar fashion, an IMBH of about 300 $M_\odot$ is generated in a lower density cluster with $W_0 = 6$, $R_h = 0.6$ pc, and $f_c = 1.0$ just with less merger of more massive stars (right-hand panel). In each panel, we indicate the time of the collision after the start of the simulation in Myr and the radius from the centre in pc. We also characterize the type interaction in the following way: **BC**: Binary collision – the two colliding objects formed a binary before the collision, **PBC**: the binary is primordial, **DBC**: the binary has formed dynamically, **HC**: hyperbolic collision, **CC**: chain collision – all collisions not classified as **DBC** or **HC**. If the two colliding objects formed a binary before coalescence the period is given in d. In the blue (black) boxes, we indicate the amount of stellar (BH) material accreted by the IMBH. Here, it is important to mention that the figure shows all collisions experienced by each participant; if an object appears in the plot only once it implies that the object never experiences any collision before.

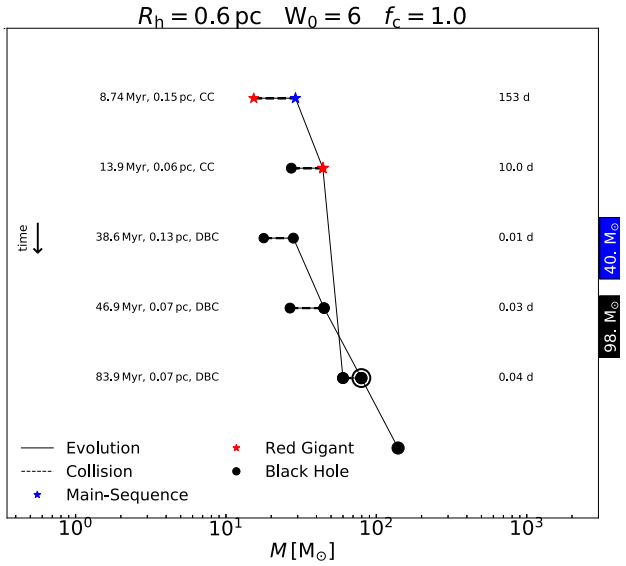

Figure 5. Formation and evolution of an IMBH in a simulation with $W_0 = 6$, $R_h = 0.6$ pc, and $f_c = 0.1$, similar to Fig. 4. However, here the BH reaches a mass of about 140 $M_\odot$ mostly through collisions (horizontal dashed lines) with other BHs. This is the only case, out of 80 simulations analysed, where a BH above 100 $M_\odot$ built up its mass mostly through collisions with other BHs.

In summary, when a single object interacts with hard binaries, the binaries tend to harden and become more massive, and they also gain angular momentum and eccentricity. For all these reasons, triple interactions drive the chain of star–star collisions leading to the formation of VMSs. They are also the main process that triggering BHs–VMSs mergers (see Fig. 7).

According to Fig. 3, the less concentrated model R06W6 and the more dense model R06W9 have comparable probability to produce IMBHs and VMSs despite the marked difference in the initial central density. Fig. 8 displays the time evolution of the core radius (plot on the top) and the core density (plot on the button) for two simulations with $W_0 = 9$ and $W_0 = 6$. The two systems experience different initial evolution: the core of the cluster with higher central density expand from the beginning of the simulation due to primordial binaries interactions, contrarily clusters with $W_0 = 6$ undergo core collapse (this is also confirmed by the evolution of the Lagrangian radii shown in the last figure of this article). Consequently, the initial concentration discrepancy between the two models rapidly decreases. This fact might explain why clusters with $W_0 = 9$ and $W_0 = 6$ lead to comparable results although the initial central densities of the two models differ of more than two orders of magnitude. On the other hand, as we will see in the next subsection, different values of the accretion factor f_c can influence the result significantly, as shown in Fig. 9.

The absence of relativistic recoil velocity does not influence the series of collisions and interactions that lead to the VMS–BH mergers. The BHs involved in these collisions are the remnant of massive stars and they did not merge with any other BH. This can be clearly seen from Figs 4 and 10. Both figures report all the collisions experienced by each object that participates in the collision chain. Therefore, if a BH appears in the plot only once it implies that the object never experiences any collision before.

The IMBHs in our simulations are mainly growing through two channels:

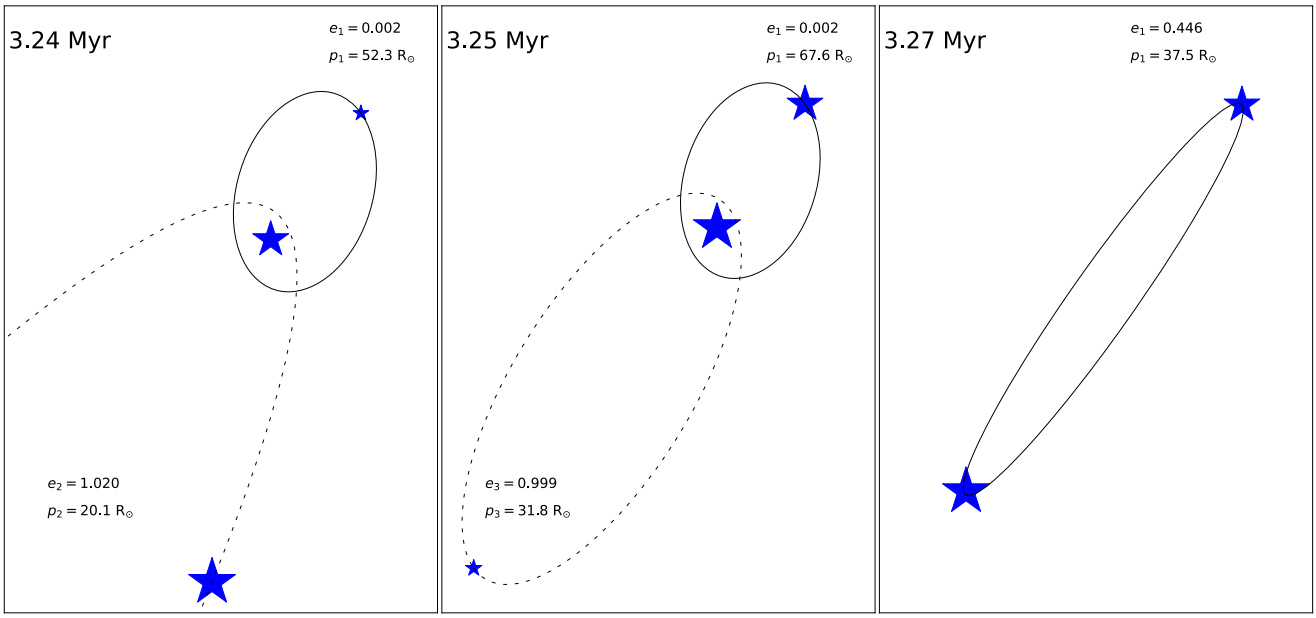

Figure 6. Sketch of the triple interaction that induces the collision of two massive stars of 170 and 80 M$_\odot$. Left-hand panel: The 170 M$_\odot$ approaches a binary in a hyperbolic orbit. Central panel: The exchange between the lightest component of the binary and the intruder of 170 M$_\odot$. Right-hand panel: The perturbed 170 and 80 M$_\odot$ binary increase its eccentricity, the two components are about to merge.

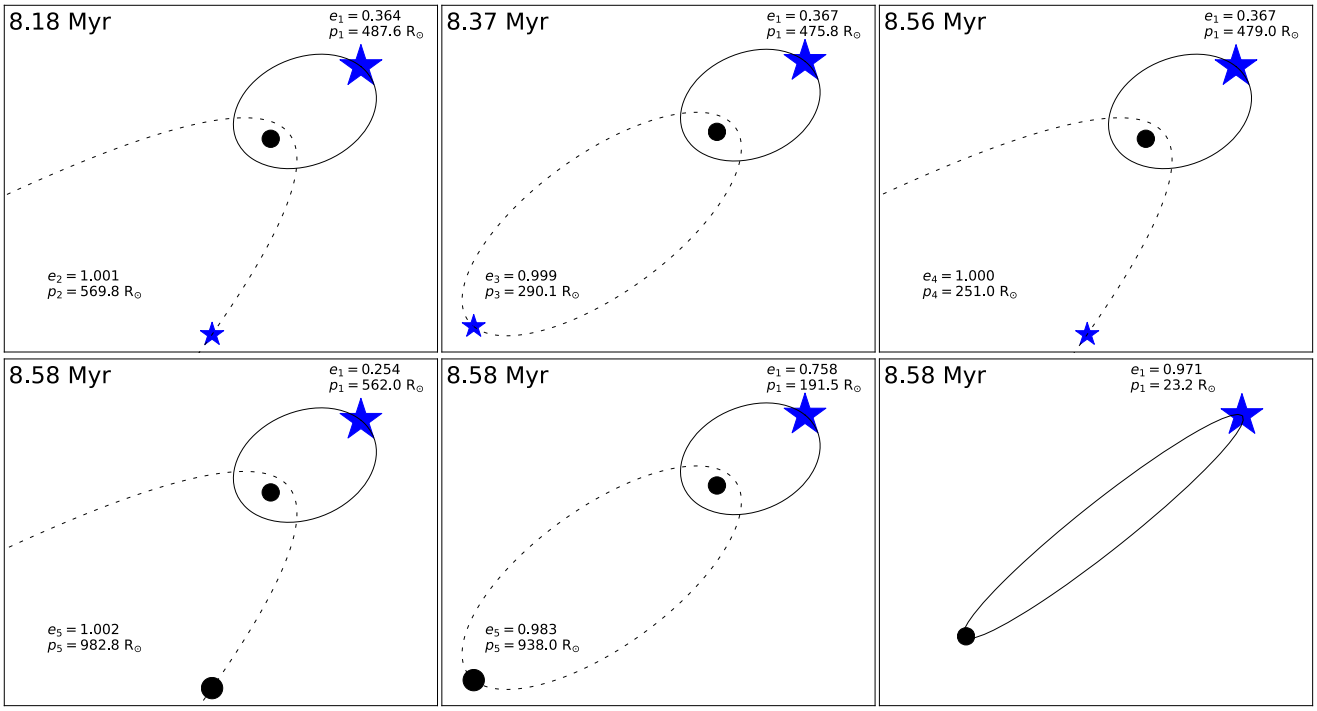

Figure 7. Sketch of the last five triple interactions experienced by a BH–VMS binary before the collision. In the last interactions, the BH–VMS binary forms a hierarchical triple with a stellar BH. Consequently, the binary increases its eccentricity to a value close to unity that leads the BH to merge with the VMS.

(i) Accretion of stellar material through binary collisions with stars, and to a lesser extent, through hyperbolic collisions with stars.
(ii) Collision with low-mass BHs.

BHs can also become more massive through multiple mass transfer events that do not lead to coalescence. However, the mass absorbed in those events is negligible. Moreover, BHs could also grow through tidal captures. However, according to our simulations, tidal captures do not seem to be relevant for the IMBHs final mass. Tidal captures are very rare (10–15 events per run) and only a small fractions of these events lead to collisions.

Collisions with stellar BHs typically add little ($\sim$ 10 to 30 per cent; see Table 1) to the total IMBH mass. BH–BH collisions are not very likely to occur. This type of binary requires very small

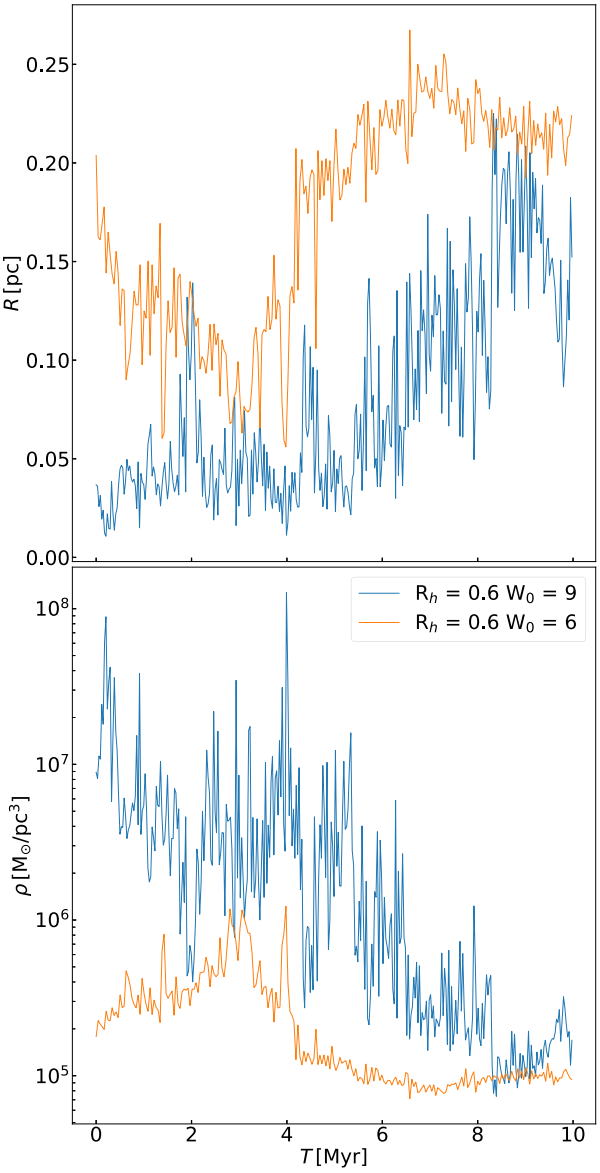

Figure 8. Time evolution of core radius (top panel) and core density (bottom panel) for two models with the same initial size $R_{\rm h} = 0.6$ pc but different initial central potential parameter W_0 (blue: R06W9, orange: R06W6). The figure shows a constant rapid expansion for the R06W9 model as opposed to an initial contraction for R06W6 simulation. The initial central density difference in the two models decreases in the first few Myr.

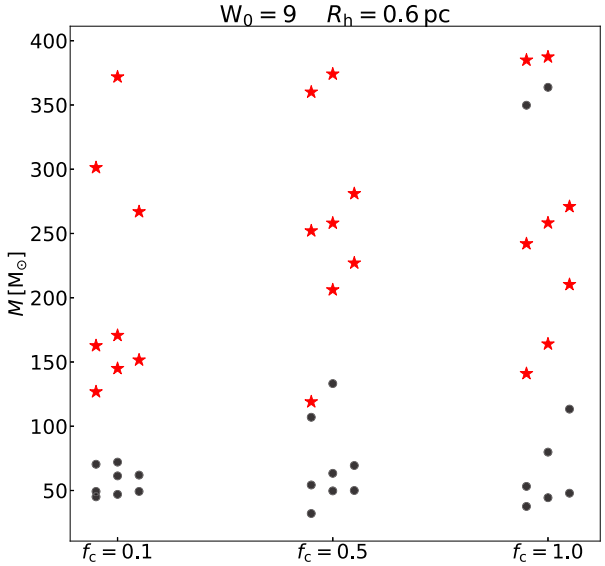

Figure 9. Comparison between R06W9, R06W9F05, and R06W9F01. Each black circle (red star) shows the mass of the most massive BH (MS star) formed in a single simulation.

semimajor axes, or very high eccentricities to enter in the post-Newtonian regime, experience gravitational wave energy loss, and eventually merge. This requires the BH binary to undergo several strong triple interactions (or binary–binary interactions). For this reason, as we can see in Fig. 4, and later also in Fig. 10, that most of the material accreted on to a massive BH originates from stars. We form in total 17 BHs with a masses above 100 $M_\odot$ (see Table 1). Despite being unlikely, one of the IMBHs grows its mass almost entirely by swallowing other BHs (as shown in Fig. 5). The formation process occurred in about ∼90 Myr and it involves a chain of low-mass BH mergers with masses of 17 : 28, 25 : 45, 68 : 70 $M_\odot$. This mechanism is particularly interesting because it provides a straightforward explanation of GW190521, the last LIGO/VIRGO detection (Abbott et al. 2020). The GW190521 gravitational signal is produced by the merger of two BHs around 66 and 85 $M_\odot$. Both masses might fall in the predicted pulsation pair-instability 'mass gap' (Woosley 2017). Our simulation indicates that collisions triggered by dynamical interactions can lead to the formation of BHs in this mass gap in agreement with (Kremer et al. 2020).

4.2 Collision fraction $f_{\rm c}$

So far we have assumed an accretion fraction of $f_{\rm c} = 1$, i.e. in star–BH collisions all stellar material is accreted on to the BH. Under these circumstances IMBHs regularly form in the simulations. However, the accretion fraction is highly uncertain (see Section 2.3 for more details). Therefore, we have simulated R06W9 with lower fractions of $f_{\rm c} = 0.5$ and $f_{\rm c} = 0.1$. The results indicate that the accretion fraction can significantly change IMBH growth (see Fig. 9). In fact, while the stars still grow in mass by collisions, no IMBH is formed in the simulation with $f_{\rm c} = 0.1$ (R06W9F01, the most massive BH has a mass of about 60 $M_\odot$). Even for simulations with $f_{\rm c} = 0.5$, just two (out of eight simulations) IMBHs form with masses only slightly above a hundred solar masses. Apart from the obvious effect that the BHs grow less in a collision with a VMS, there are also secondary effects. Less massive BHs have a higher probability to escape from the cluster after strong interactions and they have lower probabilities of experiencing additional collisions due to lower gravitational cross-sections decreasing the probability to experience close encounters.

Secondly, BH–VMS collisions with lower accretion fractions result in instantaneous mass removal from the inner part of the cluster[10] leading to cluster expansion, lower densities, and a lower merger rate. As we can see in Fig. 11, this effect is particularly enhanced in $f_{\rm c} = 0.1$ simulations because in this case when a star collides with a BH, 90 per cent of the mass of the star is instantly ejected from the cluster.

[10]In all our simulations BH–VMS collisions occur in the central region of the cluster.

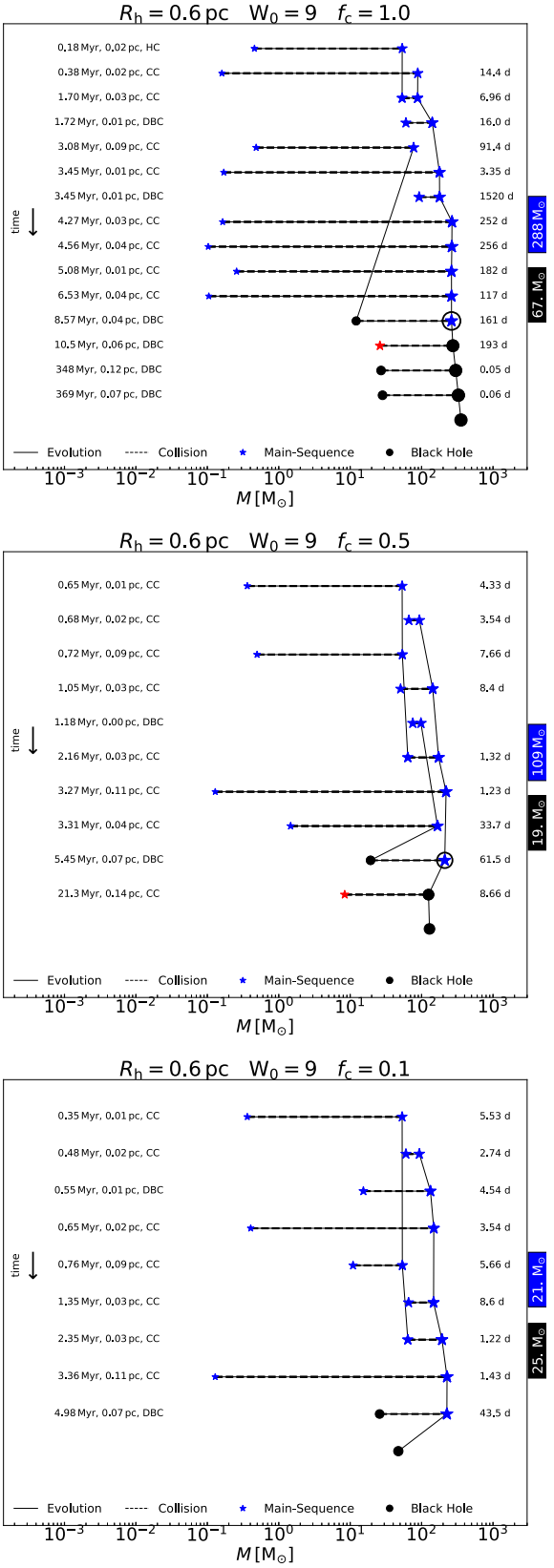

Figure 10. Comparison of three models with identical initial conditions and decreasing f_c of 1, 0.5, and 0.1 from top to bottom. For $f_c = 0.1$, no IMBH forms. The time of IMBH formation is indicated by a black circle in the two top panels. Here, we show a different realization of model R06W9 than in Fig. 4.

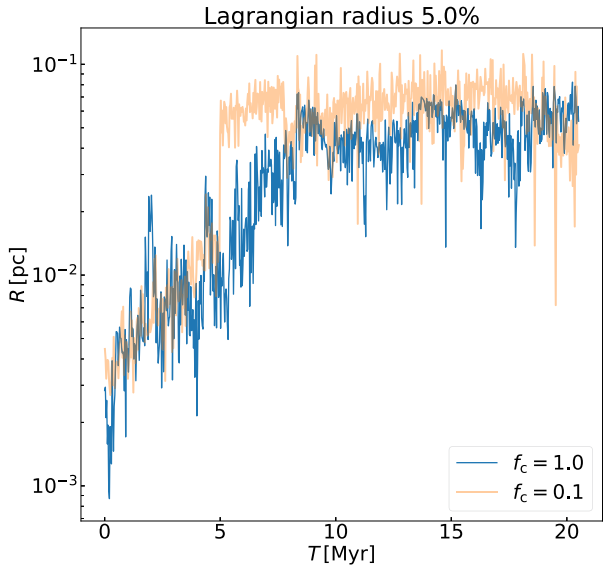

Figure 11. Comparison between 5 per cent Lagrangian radii (see Section 4.3 for the definition of Lagrangian radii) for a simulation with $f_c = 1.0$ (blue) and a simulation with $f_c = 0.1$ (orange). Observing the orange line, we can notice a fast expansion at about 5 Myr triggered by mass-loss. This dilatation is generated by a BH–VMS collision event that occurred at 4.98 Myr. During the collision, 90 per cent of the total mass of the VMS is assumed to be ejected instantly from the cluster. For simulations with $f_c = 1.0$, these type of expansions do not occur because the mass of stars is fully retained in the cluster when BH–star collisions occur.

4.3 Cluster evolution

In this section, we highlight the evolution of three different simulations resulting in very different peak BH masses, which we label, for simplicity, with S_1, S_2, and S_3. S_1 and S_2 are two different realizations of the model R06W6. The latter creates an IMBH of 140 $M_\odot$ (the evolution path of this BH is shown in Fig. 5). The most massive BH in S_1 only reaches 60 $M_\odot$. S_3 is one realization of the model R06W9 generating an IMBH, with a mass of about 350 $M_\odot$ (see evolution path in Fig. 4). The left-hand, centre, and right-hand panels in Fig. 12 refer to S_1, S_2, and S_3. respectively. Each panel consists of three plots. The plots at the top display the time evolution of the radii enclosing 3 per cent, 5 per cent, 10 per cent, 30 per cent, 50 per cent, and 70 per cent of the cumulative stellar mass (Lagrangian radii). The middle plots illustrate the evolution of the average stellar mass within 3 per cent, 5 per cent, 10 per cent, and 30 per cent Lagrangian radii. The plots at the bottom show the mass (and the type) of the most massive object in each cluster as a function of time and its distance from the cluster centre.

The evaluation of these three systems highlights the complex interplay between stellar evolution and dynamical interactions. The former has a strong impact on the early phase, while the latter plays a major role in driving the long-term change. Stellar evolution mass-loss triggers a strong expansion on early cluster evolution (Applegate 1986; Chernoff & Shapiro 1987; Chernoff & Weinberg 1990; Fukushige & Heggie 1995) Our simulations confirm these results. The 30 per cent, 50 per cent, and 70 per cent Lagrangian radii indicate a strong monotonic cluster inflation in the first ∼10 Myr as a consequence of mass-loss due to supernovae explosion and stellar winds followed by a moderate expansion driven by primordial binaries and further mass-loss due to stellar/binary evolution.

Since our three simulations are multimass systems, they undergo mass segregation in about ∼1.4 Myr (see Table 1). As a consequence

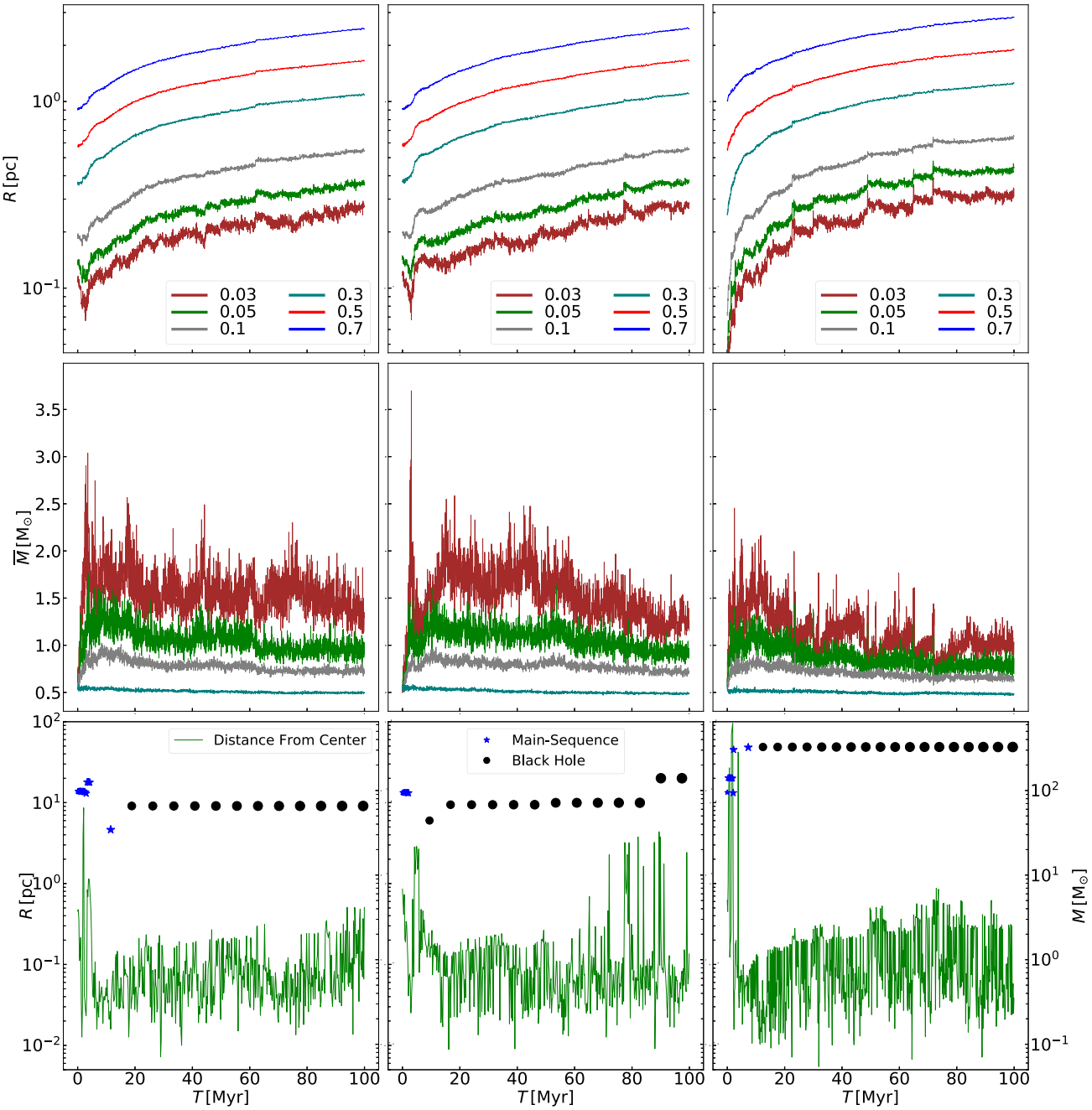

Figure 12. Lagrangian radii evolution (upper plots), particle mass average evolution (central plots), and distance and mass of the most massive object (button plots). The left-hand, central, and right-hand panels report the results of three different simulations. The simulation on the left is a realization of the R06W6 model that does not form IMBHs (the most massive BH has a mass of 60 $M_\odot$). The central panel refers to another realization of the R06W6 model that generated an IMBH of 140 $M_\odot$ through a chain of BH–BH collisions. The plots on the right report the outcome of a R06W9 realization where an IMBH of about 350 $M_\odot$ formed in a VMS–BH collision.

of that, the average stellar mass in the inner part of the three clusters strongly increases in the first ∼2 Myr (middle panels of Fig. 12). S_1 and S_2 also register an initial core collapse connected with mass segregation (rapid decrease for 3 per cent, 5 per cent, and 10 per cent Lagrangian radii) in agreement with previous numerical work (Portegies Zwart & McMillan 2002; Gürkan et al. 2004; Portegies Zwart et al. 2004; McMillan 2008). On the other hand, S_3 does not show any indication of core collapse. The system is already so dense that binary interactions prevent the collapse and force the core to expand (the innermost Lagrangian radii are in constant expansion since the beginning of the simulation. See top-right plot of Fig. 12).

Subsequently, the death of the most massive stars leads to a mass average drop in the inner part of the cluster for both S_1 and S_2 (see red line in central plots). The average mass then continues to oscillate, but while in S_1 it presents a steady decline, S_2 raises again due to a BH–BH merger after about 15 Myr. After that, it declines at a constant rate due to stellar evolution mass-loss. The initial drop is

less evident in S_3 also because the presence in the centre of the IMBH[11] compensates for the absence of the massive stars.

Massive objects located in the core of the cluster experience frequent strong interactions. This effect is reflected in the strong oscillations of the mass average in the core (see central plots) as well as the strong variations in the position of the IMBHs (see green lines in the button plots). In S_3, the IMBH oscillates in position between 0.01 and 0.5 pc with an average position of about 0.1 pc. Similarly, the BH in S_1 moves around 0.1 pc with slighter stronger oscillations due to its lower mass. On the other hand, the BH in S_2 experiences strong radial change few millions years before its coalescence with another BH at 84 Myr. These heavy oscillations are generated by the strong interactions that triggered the last BH–BH collision.

4.4 Comparison with observations

VMSs, formed through collisions between lower mass stars, appear in almost all the realizations of our 10 models. If the VMSs formation mechanism proposed in this and other works (Portegies Zwart & McMillan 2002; Gürkan et al. 2004; Portegies Zwart et al. 2004; Mapelli 2016; DiCarlo et al. 2020; Wang et al. 2020) is correct they might be observed inside or close to dense star clusters. Early studies of the Arches cluster indicated an upper star mass limit of 150 $M_\odot$ (Figer 2005). However, more recent observations indicate the existence of stars greatly exceeding this limit, suggesting the presence of VMSs up to 300 $M_\odot$ in the vicinity of YMSCs (Crowther et al. 2010). Another study claimed the discovery of a VMS of initial mass in the range between 90 and 250 $M_\odot$ in the central cluster of the region W49 (Wu et al. 2014). These stars might be generated via runaway collisions as indicated by the outcome of our and previous studied discussed in Section 5. However, gas accretion could be an equally valid mechanism for the formation of VMSs (Krumholz 2015).

It has been shown that the massive BH that power the hyperluminous source associated with MGG-11 might have a dynamical origin. The high density and compactness of this cluster allow for the formation of a few thousand solar masses star via collisional runaway, which might directly collapse into an IMBH (Portegies Zwart et al. 2004). Also, our results suggest that IMBHs could be the origin of HLXs associated with dense star clusters. It is not rare for our simulated IMBHs to accrete mass and merge with stars, as shown in the top and central plots of Fig. 10 (both plots show the IMBH merging with a red giant at 10 and 21 Myr). However, even if our results show that IMBHs do receive mass from other stars, the mass transfer events are very often interrupted by strong interactions and therefore they do not last more than 1 Myr. In other words, the IMBHs tend to spend only a small fraction of their time accreting material from their companion. This, in addition with the fact that IMBHs have a non-negligible probability to be ejected from the cluster after a BH–IMBH collision (Arca-Sedda, Amaro-Seoane & Chen 2020; Mapelli et al. 2020), might explain the absence of IMBHs accretion signature in may star clusters and most of globular clusters (Wrobel, Nyland & Miller-Jones 2015; Wrobel & Nyland 2020).

Our simulations reveal that IMBHs, right after formation, tend to bind with a low-mass BH in a BH–BH binary. The binary, located at the centre of the cluster, experiences constant gravitational interaction with other objects, and it merges in an interval of time between ∼10 and 100 Myr generating gravitational wave signal. The results also show that hierarchical BH mergers,[12] could be observed in dense stellar systems, as shown in Figs 5 and 10 (top panel), however, as pointed out in recent studies (Arca-Sedda et al. 2020; Mapelli et al. 2020) these events might be suppressed by the gravitational wave kicks. The latter were not included in our simulations although we expect them to generate a large recoil velocity especially if the two colliding BHs have comparable masses (Campanelli et al. 2007; Baker et al. 2008; Lousto & Zlochower 2009; Kulier et al. 2015; Morawski et al. 2018; Zivancev et al. 2020).

BH–IMBH coalescence, as well as the inspiral phase, will be detected by the next generation of gravitational wave detectors. Events that involve an IMBH with mass <200 $M_\odot$ should be detected by LIGO while signal generated by IMBHs with masses <2000 $M_\odot$ should be observable with the Einstein Telescope (Fragione, Ginsburg & Kocsis 2018; Arca-Sedda et al. 2020).

5 COMPARISON WITH PREVIOUS WORK

Various groups have predicted runaway merger scenario for the formation of VMSs and IMBHs in dense stellar environments. For example, direct *N*-body simulations, carried out by Portegies Zwart et al. (2004), indicate the formation of a few thousand solar masses stars produced by multiple stellar mergers. The simulated star clusters, containing 128k stars, were evolved for 12 Myr using STARLAB (Portegies Zwart et al. 2001) and NBODY4 (Aarseth 1999). The stellar evolution prescription adopted was based on Hurley et al. (2000) for stars with masses ≤50 $M_\odot$ while more massive stars follow the evolution track given by Stothers & Chin (1997) and Ishii, Ueno & Kato (1999). With these models, stars more massive than 260 $M_\odot$ collapse directly into IMBHs without losing mass in supernova explosions.

A similar mechanism is observed in the 30 simulations presented by Mapelli (2016), where VMSs reach about 500 $M_\odot$ through runaway collisions. Each of these simulations is initialized with 10^5 stars following a King density profile with $W_0 = 9$ and $R_h = 1.0$ pc. The clusters were evolved for 17 Myr using STARLAB. Due to the different stellar evolution model adopted for massive stars, these simulations generate IMBHs of few hundred solar masses through direct collapse of VMSs (the VMSs at low metallicity lose a relatively small fraction of their masses).

The analysis of the 6000 simulations of lower mass clusters presented in DiCarlo et al. (2020) shows that BHs of about 300 $M_\odot$ can form through dynamical interaction and collisions. The clusters, evolved using NBODY6++GPU, adopted the MOBSE stellar evolution (Mapelli et al. 2017; Giacobbo, Mapelli & Spera 2018). This prescription is based on Hurley et al. (2000, 2002) and it includes new prescriptions for massive stars reducing the mass-loss in supernovae explosion and stellar winds. The systems were initialized with an initial mass in the range between 10^3 and 3×10^4 $M_\odot$. The initial central densities and initial half-mass radii were computed as a function of the initial mass of the cluster.

Simulations evolved with Monte Carlo codes reveal similar outcomes. Freitag et al. (2006) computed over 100 models, varying the cluster size, particle number, and central concentration. They systematically changed the number of stars between 10^5 and 10^8 represented by a maximum of 9×10^6 particles. Their result show that 20 per cent of the clusters with an initial central potential parameter $W_0 \geq 8$ form a VMS with a mass ≥400 $M_\odot$. Other simulations

[11] In S_3, the IMBH form very fast, at about 8 Myr. On the other hand, the IMBH in S_2 is generated after 84 Myr.

[12] Multiple mergers of BHs that form more massive ones.

carried out using Monte Carlo models show that multiple VMSs can form within the same cluster (Gürkan et al. 2006).

The analysis of 2000 of simulations (Leigh et al. 2013; Giersz et al. 2015), evolved using the MOCCA (MOnte Carlo Cluster simulAtor) code, reveals the formation of IMBHs in dense stellar environment (Giersz et al. 2015). The outcome of these simulations indicates that about 20 per cent of the simulated clusters generate a BH with a mass larger than 100 $M_\odot$. These BHs have formed through collisions between a VMS and a stellar BH. The formation path is very similar to the one indicated by our *N*-body simulations (see Figs 10 and 4). However, in general, the IMBHs produced in MOCCA simulations tend to be systematically slightly more massive as the runaway main-sequence star collisions lead to more massive VMSs in than in MOCCA *N*-body. In fact, in MOCCA simulations the stellar evolution time-step is performed at the end of the relaxation time-step (that is about 10 Myr). As a consequence of that, the masses of main-sequence stars, the mass segregation, and central density are larger in the MOCCA simulations than in *N*-body simulations leading to a larger interaction rate.

The analytical work carried on by Stone et al. (2017) shows how stellar mass BHs in nuclear star clusters can grow into IMBH through runaway tidal captures of low-mass stars. As stated in their work, runaway tidal captures can be triggered only in massive and compact clusters with a velocity dispersions $\sigma > 40\,\mathrm{km\,s^{-1}}$. According to their criteria, none of our models would have made IMBHs. However, Stone et al. (2017) do not include massive stars and primordial binaries in their study, which are the key elements for the IMBH formation mechanism proposed in our work.

As we have shown in this section, the debate whether and how IMBH forms in dense star clusters is ongoing for at least two decades. Recent MOCCA Monte Carlo simulations have provided a wealth of data and answered the question positively. It is important to confirm MOCCA Monte Carlo results by direct *N*-body models, but the latter have suffered in the past from low statistical quality, if the particle number is small (say 10^4 or less), and very demanding computing time requirements, if the particle number is large (e.g. 10^5 or more). A strategy to balance low statistical quality of small *N* models has been to do larger samples of models and discuss their average (Giersz & Spurzem 1994; DiCarlo et al. 2020); but relevant astrophysical processes in star clusters (like two-body relaxation, close few body encounters, stellar evolution, tidal forces) do not scale with the same power of *N*. Therefore large sets of small *N*-body simulations can provide useful information to some degree, but can never fully substitute *N*-body simulations with more realistic larger particle numbers. Baumgardt (2017) present a very nice study using the method of small *N* samples and scaling to real star clusters; but still they are missing the effects of binaries and tidal fields, because they are difficult to scale. Our models exhibit IMBH formation in dense star clusters with an initially large particle number of more than 100k stars, 10 per cent of which are in binaries, and all relevant astrophysics; 80 such models were done using NBODY6++GPU for at least up to 300 Myr (8 models each for 10 different initial models). To our knowledge, these are so far the largest direct *N*-body simulations of their kind, and in light of the discussion above they provide the so far strongest evidence for IMBH formation.

6 SUMMARY AND DISCUSSION

We have provided evidence for the formation of IMBHs through collisions of massive stars, formation, and evolution of binaries including BHs. Debated for decades and recently underpinned by a large set of Monte Carlo (MOCCA) simulations, our direct *N*-body models are the largest and longest simulations supporting this idea of IMBH formation in dense star clusters, made possible by the use of the massively parallel GPU accelerated code NBODY6++GPU and the use of suitable supercomputers in Germany and China.

We ran and analysed 80 *N*-body simulations of compact YMSCs with different central densities (central potential parameters $W_0 = 6$, 7, 8, 9, 10) and sizes (half-mass radii $R_\mathrm{h} = 0.6$, 1.0 pc). The simulated clusters were evolved for at least 300 Myr.[13] All our models lead to the collisional formation of at least one star above 100 $M_\odot$ (the upper initial mass function limit) and several simulations create stars with masses higher than ∼400 $M_\odot$ within the first ∼10 Myr of cluster evolution. Most of the collisions were triggered by triple interactions between hard binaries and single objects. With the stellar evolution model assumed for this study, isolated massive stars cannot collapse directly into IMBHs (BHs with masses >100 $M_\odot$). Even stars with ∼500 $M_\odot$ lose most of their mass through stellar winds and collapse into a BH of about 30 $M_\odot$.

However, a sizable fraction (about 20 per cent) of our simulations result in the formation of IMBHs by means of direct collisions between stellar mass BHs and massive stars as already observed in MOCCA simulations (Giersz et al. 2015). This process is more likely in compact clusters as they form more massive stars and it takes less time for the BHs to sink into the centre. Nevertheless, if only a small fraction of the stellar mass is accreted in a collision with a BH (e.g. a collision fraction of $f_\mathrm{c} = 0.1$), the above process becomes unlikely for the formation of IMBHs in compact $\sim 7 \times 10^4\,M_\odot$ clusters investigated in this study. The value of f_c has been discussed in many theoretical (Shiokawa et al. 2015; Law-Smith et al. 2019; Bonnerot & Lu 2020; Lu & Bonnerot 2020) as well as observational studies (Wen et al. 2020). Many of these works predict f_c to be in an interval between 0.2 and 0.5. Other studies argue that $f_\mathrm{c} \leq 0.1$ might be possible (Metzger & Stone 2016). All these studies compute f_c in an SMBH–low-mass star collision event. Our case of interest involves a stellar BH colliding with a massive star; it is still poorly studied and requires future investigation.

In one simulation, the IMBH form through a series of consecutive collisions that occurred in the first ∼90 Myr (see Fig. 5). This IMBH is the final product of a merger between a 68 and a 70 $M_\odot$ BH. The 68 $M_\odot$ BH form during a collision between a 28 $M_\odot$ stellar BH and a 50 $M_\odot$ red giant (during the collision, the stellar BH absorbs the entire core of the star while the envelope is assumed to be lost). While two consecutive BH mergers 17 : 28, 25 : 45 $M_\odot$ lead to the formation of the 70 $M_\odot$ BH. The event registered in this simulation is particularly interesting because it provides a straightforward explanation of GW190521, the last LIGO/VIRGO detection (Abbott et al. 2020). The GW190521 gravitational signal is produced by the merger of two BHs around 66 and 85 $M_\odot$. Both masses might fall in the predicted pulsation pair-instability 'mass gap' (Woosley 2017), therefore they might not have had a simple stellar origin. Our simulation reveals a possible way of forming BHs with similar masses and illustrates which dynamical processes can lead to their collision.

After its formation, the IMBH can still grow moderately colliding with other low-mass BHs. Here, it is important to mention that kicks from gravitational radiation consequent to BH–BH mergers have not been implemented in our code. As a consequence of that, we might have slightly overestimated the probability for the clusters to retain

[13]The simulations that formed an IMBH of about 350 $M_\odot$ were evolved for 500 Myr.

the IMBH. However, in many cases the mass ratio involved in IMBH–BH collisions is very small ($\frac{m_{\rm BH}}{M_{\rm IMBH}} \approx \frac{20}{300} \approx 0.067$), consequently the recoil velocity should not exceed the escape velocity (Campanelli et al. 2007; Baker et al. 2008; Lousto & Zlochower 2009; Kulier et al. 2015; Morawski et al. 2018; Zivancev et al. 2020).

During the growth process of all simulations with IMBHs, with one exception shown in Fig. 5, there are no BH–BH mergers[14] before the formation of the IMBH in a VMS–stellar BH collision. Therefore, the inclusion of relativistic kicks will not change this result. After the IMBH has formed it occasionally collides with a stellar mass BH in an intermediate mass ratio inspiral event, which has the potential to kick the IMBH out of the cluster. If common, such a process might explain the missing observational evidence for IMBHs in present-day globular clusters. IMBHs might have formed in many GCs early on, and once lost, float around in the galaxies.

Adding gravitational wave kicks and spins will be possible in the future using the approximate models of Baker et al. (2008) for the kick velocity (magnitude and direction) and a new model of how initial BH spins depend on mass and metallicity by Belczynski et al. (2017). Morawski et al. (2018) have analysed large samples of BH mergers from MOCCA simulations, and show that the BH retention fraction in the cluster varies between 20 per cent and 100 per cent depending on evolutionary time and parameters of the cluster. Brem, Amaro-Seoane & Spurzem (2013) have included full post-Newtonian dynamics in their *N*-body simulation and reproduced results of Rezzolla et al. (2008), who fitted fully relativistic models. This could also be used to derive recoil velocities, in the way done by Gerosa, Hébert & Stein (2018), the latter again using fully relativistic modelling.

Our results show that the models R06W6 and R06W9, despite the difference in the initial central density, have a comparable probability to form an IMBH. The different evolution of the inner part of the clusters in these two models seems to mitigate the impact of the initial central density on the probability to form an IMBH: in very concentrated systems, the high central density forces the clusters to expand because of early energy generation by primordial binaries; on the other hand, less dense clusters undergo core collapse. Therefore, already at the very beginning of the simulation, the initial difference in central concentration between the models is reduced.

Our results indicate that compact star clusters can rapidly generate an IMBH of few hundred solar masses in about 5–15 Myr. Assuming the scenario that nuclear star clusters are generated by globular clusters that spiral towards the nucleus (Tremaine, Ostriker & Spitzer 1975), the IMBHs, if present in the clusters, can further grow in mass colliding with each other and swallowing smaller objects in the centre of the nuclear cluster (Arca-Sedda & Gualandris 2018; Arca-Sedda & Capuzzo-Dolcetta 2019; Askar, Davies & Church 2020) leading to the formation of an SMBH. This scenario is investigated by Stone et al. (2017) adopting an analytical approach. They show how low-mass BHs located in dense nuclear star cluster could rapidly grow in mass via runaway tidal captures, transforming the cluster into an SMBH.

With order 10^5 particles our models are currently the best available (in the sense of modelling all processes directly for the simulated particle number, without any scaling or averaging). However, young massive clusters in our galaxy and massive extragalactic clusters (also: nuclear star clusters) can be much more massive with particle numbers of up to 10^8 or more. NBODY6++GPU has been used for the million-body DRAGON simulations (Wang et al. 2015; Wang et al. 2016) and for million-body simulation of a nuclear star cluster (Panamarev et al. 2019). But in the first case, the central density was much lower than in this paper, so the DRAGON simulations are not prone to IMBH formation, and in the second case still, some scaling had to be used, because 10^6 particles are not enough to model nuclear star clusters. In the next ongoing studies, we are running dense star cluster models with a million bodies, and more in the future. It is feasible because only a shorter simulation time is needed (a few hundred Myr versus 12 Gyr for DRAGON). This will help us to get a better understanding of the statistics of the presence of IMBHs, not only in our Galaxy but also out to distant regions relevant for LIGO/Virgo and space-based gravitational wave detections.

The version of the code used to evolve our clusters is not based on the most updated stellar evolution recipes. Our treatment does include PISN and PPISN. Moreover, according to the adopted stellar winds prescription massive stars lose a large fraction of their initial mass. On the contrary, modern stellar winds theory (Vink et al. 2000; Gräfener & Hamann 2008; Vink et al. 2011; Sander & Vink 2020) predicts low metallicity massive stars to retain most of their masses. The most updated version of NBODY6++GPU (partly inspired by LIGO data) contains some recent stellar evolution updates[15] that include pulsation pair-instability and new treatments for stellar winds (see Belczynski et al. 2008; Banerjee et al. 2020; Banerjee 2021, for more information). This new version of the code is used for our ongoing simulations. We expect that results based on new stellar evolution prescription to be in reasonable agreement with the outcome of this paper (see Section 4.1); none of these new effects should prevent the dynamical formation mechanism of IMBHs discovered in our work; they might, however, modify the dynamical path that leads to the creation of IMBHs. Therefore, future numerical and quantitative studies in this direction are needed. In future models, we also plan to improve the modelling of the external tidal forces on the cluster, reflecting its true orbit around the host galaxy.

ACKNOWLEDGEMENTS

We acknowledge Sambaran Banerjee for the updated BSE code release before publication. FR thanks Dali University, Yunnan, China and Zhongmu Li for kind hospitality and support during a workshop in Dali in 2019 as well as National Astronomical Observatory, Chinese Academy of Sciences, Silk Road Project for hospitality during a research visits in Beijing. This work has been partly supported by Sino-German cooperation (DFG, NSFC) under project number GZ 1284, and by Chinese National Science Foundation under grant No. 11673032 (RS). TN acknowledges support from the Deutsche Forschungsgemeinschaft (DFG, German Research Foundation) under Germany's Excellence Strategy – EXC-2094 – 390783311 from the DFG Cluster of Excellence 'ORIGINS'.

The authors gratefully acknowledge the Gauss Centre for Supercomputing (GSC) e.V. (www.gauss-centre.eu) for funding this project by providing computing time through the John von Neumann Institute for Computing (NIC) on the GCS Supercomputers JURECA and JUWELS at Jülich Supercomputing Centre (JSC).

[14]In general, BH–BH collisions events are rare. This type of binaries must undergo several strong close interactions to enter the post-Newtonian regime where gravitational radiations can lead to a rapid coalescence. Because of these interactions, the binary is often ejected from the cluster before the merger occurs.

[15]These updates were made after the completion of the simulations presented in this work.

FR and RS thank Hyung Mok Lee and the Korea Astronomy and Space Science Institute (KASI) in Daejoen, Korea (Rep.), for financial support during the KCK11 meeting in 2019 December.

FR acknowledge with pleasure the helpful discussion with Francesco Flammini, Manuel Arca Sedda, and Agostino Leveque.

MG was partially supported by the Polish National Science Center (NCN) through the grant UMO-2016/23/B/ST9/02732.

RS acknowledges PKING (PKU-KIAA Innovation NSFC Group, gravitational astrophysics part, NSFC grant 11721303).

PB acknowledges support by the Chinese Academy of Sciences through the Silk Road Project at NAOC, the President's International Fellowship (PIFI) for Visiting Scientists program of CAS. RS acknowledges the National Science Foundation of China under grant No. 11673032.

LW thanks the financial support from JSPS International Research Fellow (School of Science, The university of Tokyo).

NCS received financial support from NASA, through the NASA Astrophysics Theory Research Program (Grant NNX17AK43G; PI B. Metzger). He also received support from the Israel Science Foundation (Individual Research Grant 2565/19).

This work was supported by the Deutsche Forschungsgemeinschaft (DFG, German Research Foundation) – Project-ID 138713538 – SFB 881 ('The Milky Way System'), by the Volkswagen Foundation under the Trilateral Partnerships grants No. 90411 and 97778.

The work of PB was supported under the special program of the NRF of Ukraine 'Leading and Young Scientists Research Support' – 'Astrophysical Relativistic Galactic Objects (ARGO): life cycle of active nucleus', No. 2020.02/0346.

DATA AVAILABILITY

The data underlying this article will be shared on reasonable request to the corresponding author.

REFERENCES

Aarseth S. J., 1999, PASP, 111, 1333
Abbate F., Possenti A., Ridolfi A., Freire P. C. C., Camilo F., Manchester R. N., D'Amico N., 2018, MNRAS, 481, 627
Abbott B. P. et al., 2016, Phys. Rev. Lett., 116, 241103
Abbott B. P. et al., 2017, Phys. Rev. Lett., 118, 221101
Abbott B. P. et al., 2019a, Phys. Rev. X, 9, 031040
Abbott B. P. et al., 2019b, ApJ, 882, L24
Abbott R. et al., 2020, Phys. Rev. Lett., 125, 101102
Agarwal B., Khochfar S., Johnson J. L., Neistein E., Dalla Vecchia C., Livio M., 2012, MNRAS, 425, 2854
Applegate J. H., 1986, ApJ, 301, 132
Arca-Sedda M., Capuzzo-Dolcetta R., 2019, MNRAS, 483, 152
Arca-Sedda M., Gualandris A., 2018, MNRAS, 477, 4423
Arca-Sedda M., Amaro-Seoane P., Chen X., 2020, preprint (arXiv:2007.13746)
Askar A., Davies M. B., Church R. P., 2020, preprint (arXiv:2006.04922)
Bahcall J. N., Wolf R. A., 1976, ApJ, 209, 214
Baker J. G., Boggs W. D., Centrella J., Kelly B. J., McWilliams S. T., Miller M. C., van Meter J. R., 2008, ApJ, 682, L29
Banerjee S., 2021, MNRAS, 500, 3002
Banerjee S., Belczynski K., Fryer C. L., Berczik P., Hurley J. R., Spurzem R., Wang L., 2020, A&A, 639, A41
Baumgardt H., 2017, MNRAS, 464, 2174
Baumgardt H., Hilker M., 2018, MNRAS, 478, 1520
Baumgardt H., Hut P., Makino J., McMillan S., Portegies Zwart S., 2003, ApJ, 582, L21
Baumgardt H., Sollima A., Hilker M., 2020, in Bragaglia A., Davies M., Sills A., Vesperini E., eds, Proc. IAU Symp. 351, Star Clusters: From the Milky Way to the Early Universe. Kluwer, Dordrecht, p. 400
Begelman M. C., Rees M. J., 1978, MNRAS, 185, 847
Begelman M. C., Volonteri M., Rees M. J., 2006, MNRAS, 370, 289
Belczynski K., Kalogera V., Bulik T., 2002, ApJ, 572, 407
Belczynski K., Kalogera V., Rasio F. A., Taam R. E., Zezas A., Bulik T., Maccarone T. J., Ivanova N., 2008, ApJS, 174, 223
Belczynski K., Ryu T., Perna R., Berti E., Tanaka T. L., Bulik T., 2017, MNRAS, 471, 4702
Bonnerot C., Lu W., 2020, MNRAS, 495, 1374
Brem P., Amaro-Seoane P., Spurzem R., 2013, MNRAS, 434, 2999
Brightman M. et al., 2016, ApJ, 829, 28
Campanelli M., Lousto C. O., Zlochower Y., Merritt D., 2007, Phys. Rev. Lett., 98, 231102
Casares J., Jonker P. G., 2014, Space Sci. Rev., 183, 223
Chernoff D. F., Shapiro S. L., 1987, ApJ, 322, 113
Chernoff D. F., Weinberg M. D., 1990, ApJ, 351, 121
Cohn H., 1980, ApJ, 242, 765
Colbert E. J. M., Mushotzky R. F., 1999, ApJ, 519, 89
Crowther P. A., Schnurr O., Hirschi R., Yusof N., Parker R. J., Goodwin S. P., Kassim H. A., 2010, MNRAS, 408, 731
Davies M. B., 2015, in Boffin H. M. J., Carraro G., Beccari G., eds, Astrophysics and Space Science Library, Vol. 413, Ecology of Blue Straggler Stars. Springer-Verlag, Berlin, p. 203
Davies M. B., Piotto G., de Angeli F., 2004, MNRAS, 349, 129
den Brok M. et al., 2015, ApJ, 809, 101
DiCarlo U. N. et al., 2020, MNRAS, 498, 495
Edri H., Rafter S. E., Chelouche D., Kaspi S., Behar E., 2012, ApJ, 756, 73
Eggleton P. P., Fitchett M. J., Tout C. A., 1989, ApJ, 347, 998
Eggleton P. P., Fitchett M. J., Tout C. A., 1990, ApJ, 354, 387
Farrell S. A., Webb N. A., Barret D., Godet O., Rodrigues J. M., 2009, Nature, 460, 73
Feng H., Soria R., 2011, New Astron. Rev., 55, 166
Figer D. F., 2005, Nature, 434, 192
Filippenko A. V., Ho L. C., 2003, ApJ, 588, L13
Fragione G., Ginsburg I., Kocsis B., 2018, ApJ, 856, 92
Freitag M., Rasio F. A., Baumgardt H., 2006, MNRAS, 368, 121
Fukushige T., Heggie D. C., 1995, MNRAS, 276, 206
Fürst F. et al., 2016, ApJ, 831, L14
Gebhardt K., Rich R. M., Ho L. C., 2002, ApJ, 578, L41
Gebhardt K., Rich R. M., Ho L. C., 2005, ApJ, 634, 1093
Gerosa D., Hébert F., Stein L. C., 2018, Phys. Rev. D, 97, 104049
Giacobbo N., Mapelli M., Spera M., 2018, MNRAS, 474, 2959
Gieles M., Heggie D. C., Zhao H., 2011, MNRAS, 413, 2509
Giersz M., Heggie D. C., 1994, MNRAS, 268, 257
Giersz M., Heggie D. C., 1996, MNRAS, 279, 1037
Giersz M., Spurzem R., 1994, MNRAS, 269, 241
Giersz M., Leigh N., Hypki A., Lützgendorf N., Askar A., 2015, MNRAS, 454, 3150
Gladstone J. C., 2013, Mem. Soc. Astron. Ital., 84, 629
Glebbeek E., Gaburov E., de Mink S. E., Pols O. R., Portegies Zwart S. F., 2009, A&A, 497, 255
Gräfener G., Hamann W.-R., 2008, A&A, 482, 945
Gürkan M. A., Freitag M., Rasio F. A., 2004, ApJ, 604, 632
Gürkan M. A., Fregeau J. M., Rasio F. A., 2006, ApJ, 640, L39
Heger A., Fryer C. L., Woosley S. E., Langer N., Hartmann D. H., 2003, ApJ, 591, 288
Heggie D. C., 1975, MNRAS, 173, 729
Heggie D., Hut P., 2003, The Gravitational Million-Body Problem: A Multidisciplinary Approach to Star Cluster Dynamics. Cambridge Univ. Press, Cambridge
Hobbs G., Lorimer D. R., Lyne A. G., Kramer M., 2005, MNRAS, 360, 974
Hurley J. R., Pols O. R., Tout C. A., 2000, MNRAS, 315, 543
Hurley J. R., Tout C. A., Pols O. R., 2002, MNRAS, 329, 897
Hut P., Bahcall J. N., 1983, ApJ, 268, 319
Ishii M., Ueno M., Kato M., 1999, PASJ, 51, 417

Kaaret P., Prestwich A. H., Zezas A., Murray S. S., Kim D.-W., Kilgard R. E., Schlegel E. M., Ward M. J., 2001, MNRAS, 321, L29
Kaaret P., Feng H., Roberts T. P., 2017, ARA&A, 55, 303
Kim M., López K. M., Jonker P. G., Ho L. C., Im M., 2020, MNRAS, 493, L76
King I. R., 1966, AJ, 71, 64
King A., Lasota J.-P., 2020, MNRAS, 494, 3611
Kızıltan B., Baumgardt H., Loeb A., 2017, Nature, 545, 510
Koliopanos F., 2017, Proc. Sci., XII Multifrequency Behaviour of High Energy Cosmic Sources Workshop (MULTIF2017). SISSA, Trieste, PoS#051
Kong A. K. H., 2007, ApJ, 661, 875
Kormendy J., Ho L. C., 2013, ARA&A, 51, 511
Kozai Y., 1962, AJ, 67, 591
Kremer K. et al., 2020, ApJ, 903, 45
Kroupa P., 2001, MNRAS, 322, 231
Krumholz M. R., 2015, in Vink J. S., eds, Astrophysics and Space Science Library, Vol. 412, The Formation of Very Massive Stars. Springer-Verlag, Berlin, p. 43
Kulier A., Ostriker J. P., Natarajan P., Lackner C. N., Cen R., 2015, ApJ, 799, 178
Küpper A. H. W., Maschberger T., Kroupa P., Baumgardt H., 2011, MNRAS, 417, 2300
Kustaanheimo P., Stiefel E., 1965, Crelles J., 71, 276
Lahén N., Naab T., Johansson P. H., Elmegreen B., Hu C.-Y., Walch S., 2019, ApJ, 879, L18
Law-Smith J., Guillochon J., Ramirez-Ruiz E., 2019, ApJ, 882, L25
Lee H. M., 1987, ApJ, 319, 801
Lee H. M., Ostriker J. P., 1986, ApJ, 310, 176
Leigh N., Giersz M., Webb J. J., Hypki A., De Marchi G., Kroupa P., Sills A., 2013, MNRAS, 436, 3399
Lidov M. L., 1962, Planet. Space Sci., 9, 719
Liu J.-F., Bregman J. N., Bai Y., Justham S., Crowther P., 2013, Nature, 503, 500
Lousto C. O., Zlochower Y., 2009, Phys. Rev. D, 79, 064018
Lu W., Bonnerot C., 2020, MNRAS, 492, 686
Luo Y., Shlosman I., Nagamine K., Fang T., 2020, MNRAS, 492, 4917
Lützgendorf N. et al., 2013, A&A, 552, A49
Lynden-Bell D., 1999, Phys. A, 263, 293
Lynden-Bell D., Wood R., 1968, MNRAS, 138, 495
McCrady N., Gilbert A. M., Graham J. R., 2003, ApJ, 596, 240
McMillan S. L. W., 2008, Class. Quantum Gravity, 25, 114007
McMillan S. L. W., Hut P., 1996, ApJ, 467, 348
Madau P., Rees M. J., 2001, ApJ, 551, L27
Mapelli M., 2016, MNRAS, 459, 3432
Mapelli M., Giacobbo N., Ripamonti E., Spera M., 2017, MNRAS, 472, 2422
Mapelli M., Santoliquido F., Bouffanais Y., Arca Sedda M., Giacobbo N., Artale M. C., Ballone A., 2020, preprint (arXiv:2007.15022)
Mardling R. A., 1996, in Wijers R. A. M. J., Davies M. B., Tout C. A., eds, Evolutionary Processes in Binary Stars. Springer, Cham, p. 81
Mardling R. A., Aarseth S. J., 2001, MNRAS, 321, 398
Matsumoto H., Tsuru T. G., 1999, PASJ, 51, 321
Matsumoto H., Tsuru T. G., Koyama K., Awaki H., Canizares C. R., Kawai N., Matsushita S., Kawabe R., 2001, ApJ, 547, L25
Mengel S., Tacconi-Garman L. E., 2007, A&A, 466, 151
Metzger B. D., Stone N. C., 2016, MNRAS, 461, 948
Mezcua M., 2017, Int. J. Mod. Phys. D, 26, 1730021
Mezcua M., Roberts T. P., Sutton A. D., Lobanov A. P., 2013, MNRAS, 436, 3128
Mezcua M., Roberts T. P., Lobanov A. P., Sutton A. D., 2015, MNRAS, 448, 1893
Mikkola S., Aarseth S. J., 1998, New Astron., 3, 309
Moe M., Di Stefano R., 2017, ApJS, 230, 15
Morawski J., Giersz M., Askar A., Belczynski K., 2018, MNRAS, 481, 2168
Nash P. E., Monaghan J. J., 1978, MNRAS, 184, 119
Nitadori K., Aarseth S. J., 2012, MNRAS, 424, 545
Noyola E., Gebhardt K., Bergmann M., 2008, ApJ, 676, 1008
Noyola E., Gebhardt K., Kissler-Patig M., Lützgendorf N., Jalali B., de Zeeuw P. T., Baumgardt H., 2010, ApJ, 719, L60
Oppenheimer J. R., Snyder H., 1939, Phys. Rev., 56, 455
Panamarev T., Just A., Spurzem R., Berczik P., Wang L., Arca Sedda M., 2019, MNRAS, 484, 3279
Pasham D. R., Strohmayer T. E., Mushotzky R. F., 2014, Nature, 513, 74
Patruno A., Portegies Zwart S., Dewi J., Hopman C., 2006, MNRAS, 370, L6
Peters P. C., Mathews J., 1963, Phys. Rev., 131, 435
Peterson R. C., Seitzer P., Cudworth K. M., 1989, ApJ, 347, 251
Peterson B. M. et al., 2006, ApJ, 641, 638
Pooley D., Rappaport S., 2006, ApJ, 644, L45
Portegies Zwart S. F., McMillan S. L. W., 2002, ApJ, 576, 899
Portegies Zwart S. F., McMillan S. L. W., Hut P., Makino J., 2001, MNRAS, 321, 199
Portegies Zwart S. F., Baumgardt H., Hut P., Makino J., McMillan S. L. W., 2004, Nature, 428, 724
Portegies Zwart S. F., McMillan S. L. W., Gieles M., 2010, ARA&A, 48, 431
Press W. H., Teukolsky S. A., 1977, ApJ, 213, 183
Quinlan G. D., Shapiro S. L., 1987, ApJ, 321, 199
Quinlan G. D., Shapiro S. L., 1989, ApJ, 343, 725
Quinlan G. D., Shapiro S. L., 1990, ApJ, 356, 483
Remillard R. A., McClintock J. E., 2006, ARA&A, 44, 49
Rezzolla L., Barausse E., Dorband E. N., Pollney D., Reisswig C., Seiler J., Husa S., 2008, Phys. Rev. D, 78, 044002
Roberts T. P., Middleton M. J., Sutton A. D., Mezcua M., Walton D. J., Heil L. M., 2016, Astron. Nachr., 337, 534
Ryu T., Tanaka T. L., Perna R., Haiman Z., 2016, MNRAS, 460, 4122
Sana H. et al., 2012, Science, 337, 444
Sander A. A. C., Vink J. S., 2020, MNRAS, 499, 873
Shiokawa H., Krolik J. H., Cheng R. M., Piran T., Noble S. C., 2015, ApJ, 804, 85
Smith N., Tombleson R., 2015, MNRAS, 447, 598
Spitzer L., 1987, Dynamical Evolution of Globular Clusters. Princeton Univ. Press, Princeton, NJ
Spitzer L. Jr., Hart M. H., 1971, ApJ, 164, 399
Spurzem R., 1999, J. Comput. Appl. Math., 109, 407
Stone N. C., Küpper A. H. W., Ostriker J. P., 2017, MNRAS, 467, 4180
Stothers R. B., Chin C.-w., 1997, ApJ, 489, 319
Strohmayer T. E., Mushotzky R. F., 2003, ApJ, 586, L61
Takekawa S., Oka T., Iwata Y., Tsujimoto S., Nomura M., 2020, ApJ, 890, 167
Tout C. A., Aarseth S. J., Pols O. R., Eggleton P. P., 1997, MNRAS, 291, 732
Tremaine S. D., Ostriker J. P., Spitzer L. J., 1975, ApJ, 196, 407
van den Bosch R., de Zeeuw T., Gebhardt K., Noyola E., van de Ven G., 2006, ApJ, 641, 852
Vink J. S., de Koter A., Lamers H. J. G. L. M., 2000, A&A, 362, 295
Vink J. S., Muijres L. E., Anthonisse B., de Koter A., Gräfener G., Langer N., 2011, A&A, 531, A132
Volonteri M., 2010, A&AR, 18, 279
Wang L., Spurzem R., Aarseth S., Nitadori K., Berczik P., Kouwenhoven M. B. N., Naab T., 2015, MNRAS, 450, 4070
Wang L. et al., 2016, MNRAS, 458, 1450
Wang L., Kroupa P., Takahashi K., Jerabkova T., 2020, MNRAS, 491, 440
Webster B. L., Murdin P., 1972, Nature, 235, 37
Wen S., Jonker P. G., Stone N. C., Zabludoff A. I., Psaltis D., 2020, ApJ, 897, 80
Woosley S. E., 2017, ApJ, 836, 244
Woosley S. E., Heger A., 2015, in Vink J. S., ed., Astrophysics and Space Science Library, Vol. 412, Very Massive Stars in the Local Universe. Springer-Verlag, Berlin, p. 199
Wrobel J. M., Nyland K. E., 2020, ApJ, 900, 134
Wrobel J. M., Nyland K. E., Miller-Jones J. C. A., 2015, AJ, 150, 120
Wu S. W., Bik A., Henning T., Pasquali A., Brand ner W., Stolte A., 2014, A&A, 568, L13
Zivancev C., Ostriker J., Küpper A. H. W., 2020, MNRAS, 498, 3807

This paper has been typeset from a TEX/LATEX file prepared by the author.